© 2020. Published by The Company of Biologists Ltd | Journal of Cell Science (2020) 133, jcs250837. doi:10.1242/jcs.250837

RESEARCH ARTICLE

Amalgam regulates the receptor tyrosine kinase pathway through Sprouty in glial cell development in the *Drosophila* larval brain

Majd M. Ariss[1], Alexander R. Terry[1], Abul B. M. M. K. Islam[2], Nissim Hay[1] and Maxim V. Frolov[1,*]

ABSTRACT

The receptor tyrosine kinase (RTK) pathway plays an essential role in development and disease by controlling cell proliferation and differentiation. Here, we profile the *Drosophila* larval brain by single-cell RNA-sequencing and identify *Amalgam* (*Ama*), which encodes a cell adhesion protein of the immunoglobulin IgLON family, as regulating the RTK pathway activity during glial cell development. Depletion of Ama reduces cell proliferation, affects glial cell type composition and disrupts the blood–brain barrier (BBB), which leads to hemocyte infiltration and neuronal death. We show that Ama depletion lowers RTK activity by upregulating Sprouty (Sty), a negative regulator of the RTK pathway. Knockdown of Ama blocks oncogenic RTK signaling activation in the *Drosophila* glioma model and halts malignant transformation. Finally, knockdown of a human ortholog of Ama, LSAMP, results in upregulation of SPROUTY2 in glioblastoma cell lines, suggesting that the relationship between Ama and Sty is conserved.

KEY WORDS: *Drosophila*, Receptor tyrosine kinase, Blood–brain barrier, Sprouty, Single-cell RNA-sequencing, LSAMP

INTRODUCTION

The receptor tyrosine kinase (RTK) pathway regulates growth, cell proliferation, differentiation and survival, and therefore has a prominent role in development and in cancer (Regad, 2015). Signaling through this pathway is mediated by cell surface receptors that are activated and dimerized upon binding to growth factors and that propagate signals through the RAS-RAF-MEK-ERK axis. The RTK pathway is tightly regulated at multiple levels including inhibition by members of the Sprouty gene family. This type of inhibition, measured by a decrease in ERK phosphorylation, occurs when Sprouty binds to either GRB2 or RAF and disrupts the propagation of the signal (Masoumi-Moghaddam et al., 2014). However, beyond this classical role of binding to different components of the RTK pathway, the mechanism of Sprouty repression and its regulation is not fully understood (Masoumi-Moghaddam et al., 2014). Notably, Sprouty is a potential therapeutic target in many neurological diseases (Hausott and Klimaschewski, 2019) and has been shown to act either as a tumor suppressor or as an oncogene in different cancers (Masoumi-Moghaddam et al., 2014). The latter suggests that the function of Sprouty and its impact on RTK signaling is likely cell type dependent, which further complicates investigation of the role of Sprouty in cancer given high heterogeneity in tumors.

Recent advances in single-cell RNA-sequencing (scRNA-seq) allow characterization of cell diversity at a high resolution and help to dissect cellular heterogeneity. This technology enabled identification of novel biomarkers in cell types as well as the discovery of rare cell subtypes that would have otherwise been missed in bulk RNA-seq (Papalexi and Satija, 2018). Additionally, scRNA-seq has been shown to uncover dynamic spatiotemporal processes such as differentiation (Wagner et al., 2016) and complex cell-to-cell responses following stimuli (Liu and Trapnell, 2016).

Drosophila has proven to be a highly advantageous model to study signaling pathways given its amenability to genetic analysis and remarkable conservation of signal transduction pathways between humans and flies (Chatterjee and Deng, 2019). This is best illustrated by pioneering studies of the RTK signaling in *Drosophila* (Simon et al., 1991) leading to discovery of several members of the pathway that are preserved across species (Perrimon, 1994). For instance, Sprouty was initially discovered in *Drosophila* (Hacohen et al., 1998) and it was later found to have a similar role in mammals (Impagnatiello et al., 2001). *Drosophila* has also been instrumental in studying cancers as several fly tumor models of the lung (Levine and Cagan, 2016), eye (Pagliarini and Xu, 2003), blood (Osman et al., 2009), glia (Read et al., 2009) and colon (Bangi et al., 2016) cancers have recently been established. In the *Drosophila* third-instar larva, developing glia present an ideal model to study the role of Sprouty as multiple RTK surface receptors have been shown to affect glia proliferation and migration as well as fly locomotion (Read, 2018; Avet-Rochex et al., 2012; Franzdóttir et al., 2009; Ray et al., 2017). Glial cells are also a vital component of the nervous system as they provide support and nutrition to neurons. Moreover, surface glia, which surround the nervous system, form a continuous dynamic membrane called the blood–brain barrier (BBB), which protects neurons from the high solute content of the hemolymph and prevents neurodegeneration (Bainton et al., 2005; Yildirim et al., 2019).

Here, we employed scRNA-seq to identify *Amalgam* (*Ama*), a member of the IgLON family encoding a cell adhesion immunoglobulin, as a new regulator of the RTK pathway that acts through *sprouty* (*sty*). Depletion of Ama decreases glial cell proliferation, disrupts the BBB and results in a dramatic increase of hemocyte infiltration in the brain. We show that knockdown of Ama increases Sty levels, which reduces RTK signaling pathway in glia during development and in a *Drosophila* glioma model. Notably, the impact of knockdown of Ama on Sty is conserved in human glioblastoma cell lines, suggesting a functional conservation across species.

[1]Department of Biochemistry and Molecular Genetics, College of Medicine, University of Illinois at Chicago, Chicago, IL 60607, USA. [2]Department of Genetic Engineering and Biotechnology, University of Dhaka, Dhaka, 1000, Bangladesh.

*Author for correspondence (mfrolov@uic.edu)

M.M.A., 0000-0001-8013-5172; A.R.T., 0000-0003-4731-8537; A.B.M.M.K.I., 0000-0002-7274-0855; N.H., 0000-0002-6245-3000; M.V.F., 0000-0003-3953-3739

Handling Editor: Giampietro Schiavo
Received 26 June 2020; Accepted 24 August 2020

Journal of Cell Science (2020) 133, jcs250837. doi:10.1242/jcs.250837

RESULTS

Ama is required for glial cell development

RTK signaling has been extensively studied in the *Drosophila* eye, but primarily during the context of photoreceptor differentiation and less so in the glial cells, called wrapping glia (WG), that envelope axonal projections. This glial cell type differentiates from perineurial glia (PG) as PG are migrating from the brain towards the developing eye disc during the third-instar larval stage. It has been shown that a transient increase in RTK signaling is required during the transition from perineurial to wrapping glia (Franzdóttir et al., 2009).

In order to identify novel genes important in this process, we examined the scRNA-seq dataset of the larval eye imaginal disc (Ariss et al., 2018) to isolate genes that are specifically expressed in the perineurial and wrapping glia. *Amalgam* (*Ama*) was found to be one of the top gene markers expressed in glial cells (Fig. 1A) with a higher expression in wrapping glia than in perineurial glia (Fig. S1A,B), which parallels the transient increase in RTK signaling during this transition. Ama is an adhesion protein of the immunoglobulin superfamily (Seeger et al., 1988) and affects axon pathfinding in *Drosophila* embryos (Fremion et al., 2000). To determine whether *Ama* is important in glia, we employed the *UAS-Gal4* system to knockdown *Ama* by RNAi using a *UAS-Ama*^{RNAi} transgene driven by a pan-glial *repo-Gal4* driver or a subperineurial glia (SPG) specific *moody-Gal4* driver. Depletion of *Ama* in all glial cells *repo-Gal4* resulted in early pupal lethality (~24 h after pupa formation), indicating that *Ama* could have an essential role in development. This result was validated with another *UAS-Ama*^{RNAi} transgene, thus, confirming the specificity of RNAi knockdown (Fig. S1C).

We began the investigation of the function of Ama in glia by confirming its glial-specific expression. *repo-Gal4 UAS-mCD8-GFP* eye discs, which express GFP in glial cell membranes, were dissected and subjected to a fluorescence *in situ* hybridization (FISH) protocol using *Ama*-specific Stellaris probes. As shown in Fig. 1B, *Ama* transcripts were detected exclusively in GFP-positive glial cells. In a complementary approach, the expression of *Ama* was examined by immunofluorescence using an *Ama-Gal4* enhancer trap line crossed to *UAS-GFP*, while glial cells were visualized with pan-glial Repo antibody. In agreement with the FISH results, Ama (GFP positive) was detected only in glial cells (Fig. 1C). Notably, the intensity of the GFP signal was higher in wrapping glia than in perineurial glia. Indeed, the more-intense GFP signal colocalized with Cut, a wrapping glia marker that is not expressed in perineurial glia (Fig. S1B). We also noticed that *Ama* is expressed in a subset of cells of the ventral peripodial membrane epithelium (VPE), as also revealed in the scRNA-seq dataset (Fig. S1D,E). These results suggest that the expression of *Ama* is primarily restricted to glial cells, with wrapping glia expressing a higher level of *Ama* than perineurial glia.

Since perineurial glial cells originate in the brain before migrating towards the eye disc, we examined the expression of *Ama* in the third-instar larval brain using a G-TRACE cell lineage tracing system (Evans et al., 2009). This technique provides a visual representation of temporal gene expression, labeling cells that expressed *Ama* in the past with GFP, while RFP labels cells that currently express *Ama*. With the exception of a few cells, *Ama* was almost exclusively detected in glia, based on the colocalization with Repo (Fig. 1D). Notably, every glial cell that expressed RFP also expressed GFP indicating that *Ama* remains expressed in the same cell throughout development and is not turned off (Fig. 1D). Individual confocal sections show that *Ama* is expressed in most types of glial cells but was largely absent in the medulla region of the optic lobe (Fig. S1F). Interestingly, only half of glial cells expressed *Ama* (Fig. 1E). The glial-specific *Ama* expression was further confirmed by FISH (Fig. 1F). Importantly, the signal was lost when *Ama* was depleted by RNAi using *repo-Gal4* (Fig. 1F).

To characterize the consequences of glia-specific Ama knockdown, the *repo>Ama*^{RNAi} eye discs were stained with Repo antibody to visualize glial cells. Strikingly, no glial cells were found in *repo>Ama*^{RNAi} eye discs (Fig. 1G). Since glial cells play a crucial role in photoreceptor axon guidance (Xie et al., 2014), we examined axons in the brain using a 24B10 antibody. In the wild type, axonal projections were found in the lamina and medulla of the optic lobe; however, axons failed to land in their respective compartments in the brains when glial cells were depleted of *Ama* (Fig. 1H). Furthermore, there was a severe reduction in the number of glial cells in the *repo>Ama*^{RNAi} brain and its size of was significantly smaller (Fig. 1I).

Thus, we conclude that *Ama* is essential for glial cell development. Ama depletion results in severe reduction of glia in the brain and prevents migration of glial cells from the brain towards the eye disc.

Profiling of *Ama*-depleted glia by scRNA-seq

To precisely characterize the impact of *Ama* depletion on different glial cell types in the larval brain we employed scRNA-seq. A total of 45 brains across four biological replicates in each of the *repo>+* and *repo>Ama*^{RNAi} larva were dissected and then dissociated into a single-cell suspension to perform scRNA-seq through the Drop-seq technique (Macosko et al., 2015) (Fig. 2A). Following sequencing alignment and digital expression matrix generation, the Seurat v3.0 package (Stuart et al., 2019) was used to normalize and filter out the low-quality cells. In wild type, 16,553 high-quality cells were retained. These cells were grouped into 17 distinct clusters based on similarity in gene expression, and the clustering was visualized through a uniform manifold approximation and projection (UMAP) algorithm. Cells in each cluster are characterized by a specific list of expressed genes or biomarkers (Fig. S2A,B; Tables S1, S2). The neuronal cell clusters were identified based on the neuronal marker *elav*, whereas the glial clusters were identified by *repo* expression (Fig. S2A; Table S2). Glial cell clusters were selected for further analysis.

There are multiple types of glial cells in the developing third-instar larval brain. Surface glia (SG), consisting of perineurial glia and subperineurial glial cells, are situated at the surface of the third-instar larval brain and form the BBB (Bainton et al., 2005). The barrier protects neurons from degeneration and the acidic environment of hemolymph. There are two types of neuropil-associated glia (NP), astrocyte-like glia (AG) and ensheathing glia (EG), which infiltrate and cover neuropils, respectively, in the central brain and optic lobe (Omoto et al., 2015). Cortex glia (CG) encase neurons and are located between SG and the neuropils (Pereanu et al., 2007). Finally, glia progenitor cells (GPCs) are situated between the lamina neuropil and SG of the optic lobe and give rise to glia in the optic lobe (Yoshida et al., 2005).

The supervised analysis of glial cells selected based on *repo* expression encompassed 760 cells across nine clusters. The distinct marker list in each cluster was used to assign and label the different glial cell types based on previously published work (Fig. S3A–C; Tables S3 and S4). Thus, cells of GPC, SG, NP, WG cell types were readily identified. Interestingly, cells of the Fasciclin (Fas) cluster express markers of multiple glial cell types. For instance, *Fas2* and *alrm*, which are highly expressed in the Fas cluster, are surface and

Journal of Cell Science (2020) 133, jcs250837. doi:10.1242/jcs.250837

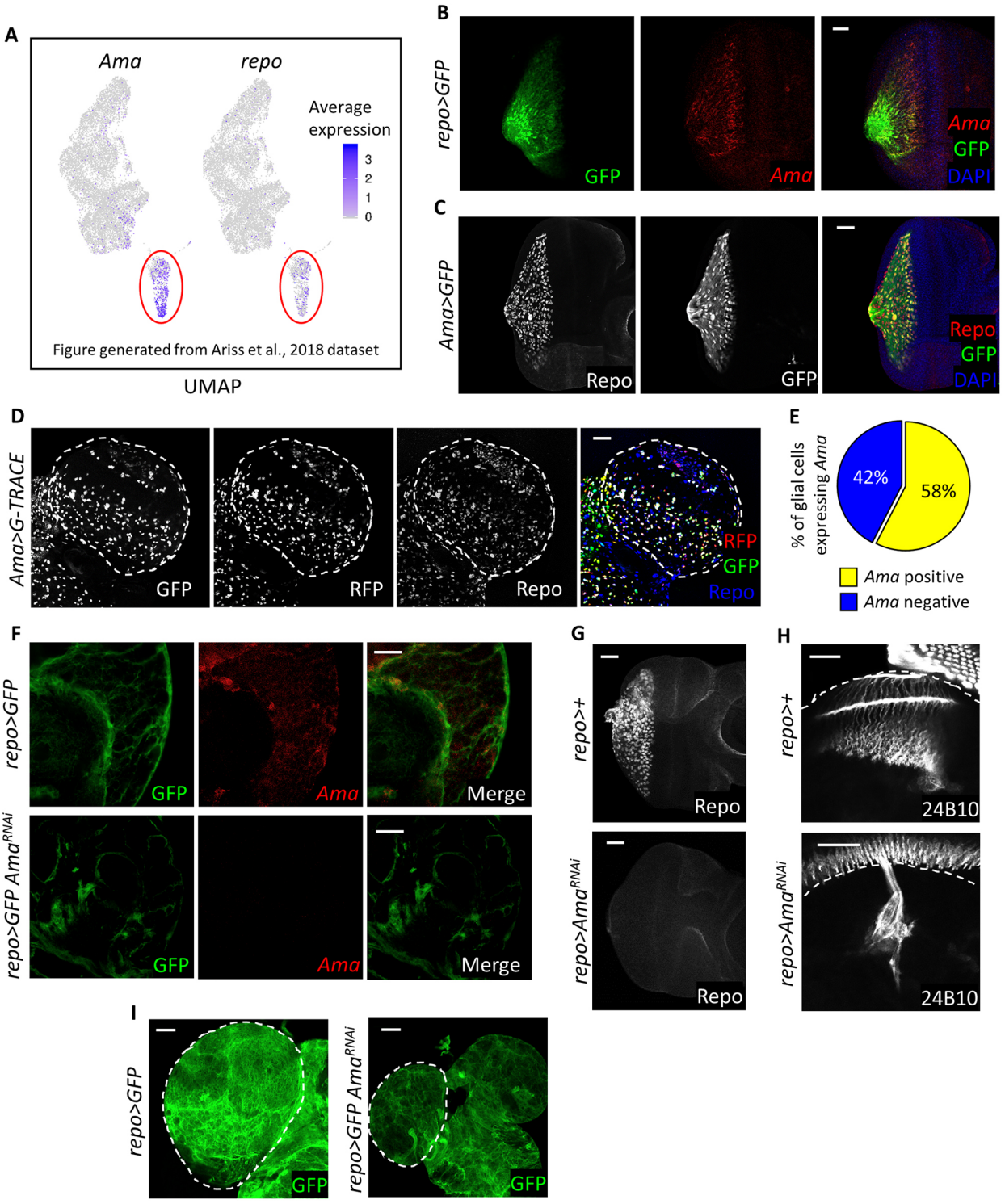

Fig. 1. *Ama* is expressed in glia and is required in glial development. (A) Feature plots displaying the expression of genes on the UMAP clusters of a previously published third-instar eye disc scRNA-seq dataset (Ariss et al., 2018), showing that *Ama* and *repo* are co-expressed in the same cluster. (B) FISH for *Ama* mRNA in the eye disc showing expression in glial cells with glial membranes labeled by GFP. Final genotype: *repo>mCD8GFP*. (C) Repo immunofluorescence in the eye disc displaying expression in *Ama*-positive cells labeled by GFP. (D) Repo immunofluorescence in the third-instar brain (dashed outline) of *Ama>G-TRACE* showing the lineage and real-time expression of *Ama-Gal4*. GFP labels the lineage, whereas RFP represents the real-time expression. (E) Pie chart outlying the percentage of glial cells expressing *Ama*. *Z*-stacks of *Ama>G-TRACE* brains were counted. Data represent means of three experiments (Table S8). (F) FISH for *Ama* mRNA in the brain showing that there is expression in glial cells, with glial membranes labeled by GFP. Knockdown of Ama in glia results in loss of the FISH signal. Final genotypes: *repo>mCD8GFP* (top panel) *repo>mCD8GFP Ama^{RNAi}* (bottom panel). (G) Repo immunofluorescence shows the lack of glia in the eye disc following Ama depletion. (H) Immunofluorescence using 24B10 antibody to label photoreceptor axons indicates defects in axons guidance in *repo>Ama^{RNAi}*. The dashed lines indicate the outline of the brain. (I) Brains (outlined by dashed lines) are smaller in *repo>Ama^{RNAi}* than in *repo>GFP*. GFP labels glial cell membranes. Final genotypes: *repo>mCD8GFP* (left panel) *repo>mCD8GFP Ama^{RNAi}* (right panel). Scale bars: 20 µm.

Journal of Cell Science (2020) 133, jcs250837. doi:10.1242/jcs.250837

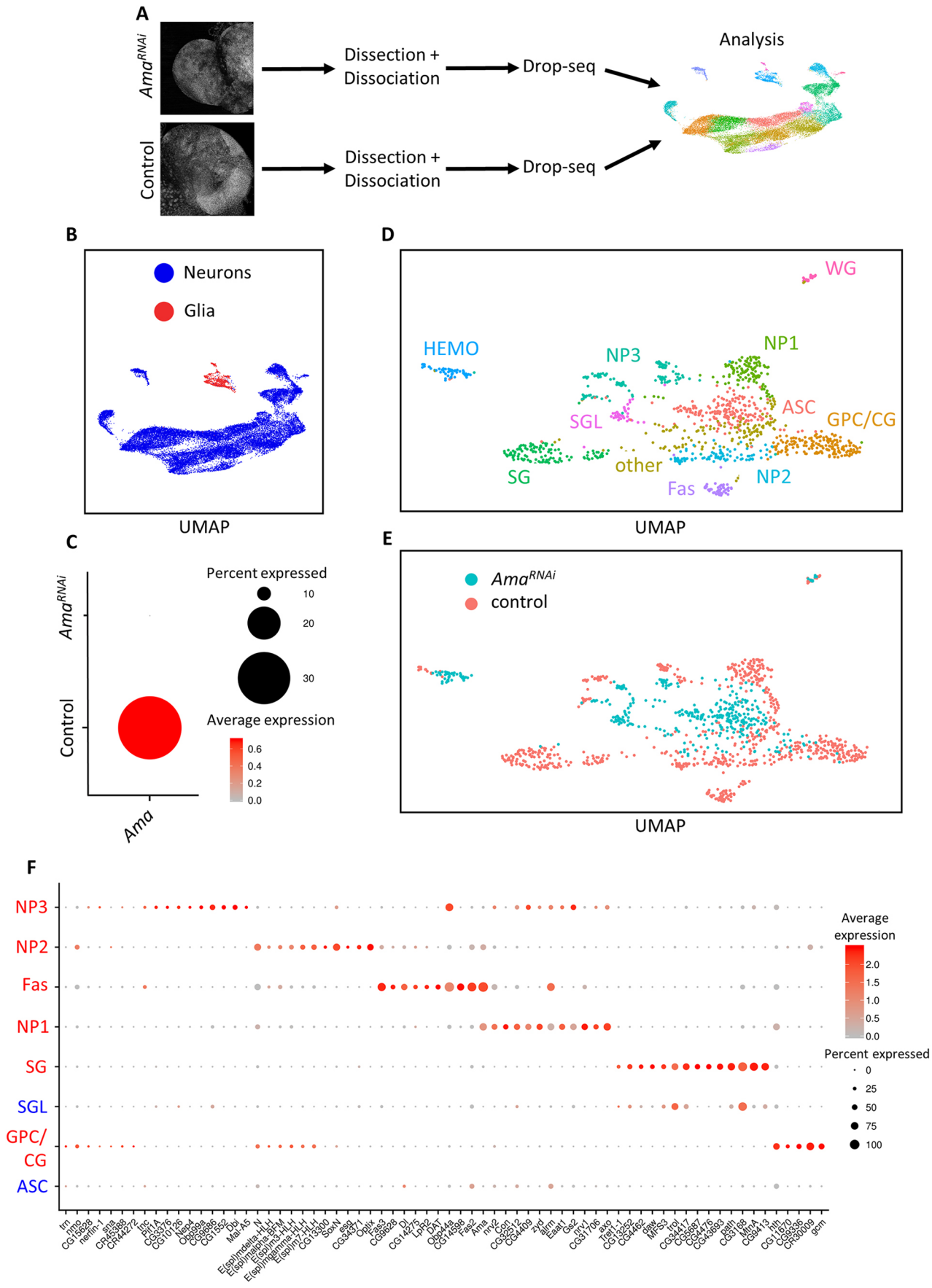

Fig. 2. See next page for legend.

Journal of Cell Science

Journal of Cell Science (2020) 133, jcs250837. doi:10.1242/jcs.250837

Fig. 2. scRNA-seq identifies cellular perturbations following Ama knockdown. (A) Illustration of scRNA-seq pipeline. Third-instar larval brains from Control (*repo*>+) and *Ama*^{RNAi} (*repo*>*Ama*^{RNAi}) were dissected then dissociated into a single-cell suspension. Drop-seq was performed to capture single cells and generate cDNA libraries. Following alignment and generating a single-cell gene expression matrix, the samples were analyzed using Seurat to unbiasedly find cell clusters having distinct gene expression profiles. (B) UMAP of 25,700 cells outlying the neuronal and glial cells from the combined *repo*>+ (16,553 cells) and *repo*>*Ama*^{RNAi} (9147 cells) scRNA-seq brains. (C) Dot plot in *repo*>+ and *repo*>*Ama*^{RNAi} brains displaying the depletion of *Ama* expression using scRNA-seq. The red color represents the average expression of *Ama* (average log fold change), whereas the size of the dot represents the percentage of cells expressing *Ama*. (D) UMAP from the supervised analysis on glial cells from *repo*>+ and *repo*>*Ama*^{RNAi} brains displaying ten distinct clusters. GPC/CG, glia precursor cells/cortex glia; ASC, *Ama*^{RNAi} specific cluster; SG, surface glia; SGL, surface glia-like; NP1, neuropil glia 1; NP2, neuropil glia 2; NP3=neuropil glia 3; Fas, fasciclin cluster. (E) UMAP from D showing the genotype of each cell. (F) Dot plot displaying the top markers in different clusters from the analysis in D. The red color gradient shows the average expression of the genes (average log fold change), whereas the dot size shows the percentage of cells in the cluster expressing the gene. ASC glia do not share markers of other control glial cluster. SGL share markers with SG cells. Clusters labeled in red are observed in the *repo*>+ supervised glial analysis. Clusters labeled in blue are additional clusters that appeared after pooling *repo*>+ cells with *repo*>*Ama*^{RNAi} brains. HEMO and WG are excluded as they originate from the hemolymph and the peripheral nervous system, respectively, and not the brain. In this analysis, GPC and CG results were pooled.

neuropil glia markers, respectively (DeSalvo et al., 2014; Doherty et al., 2009). Moreover, *Ama* is also expressed in multiple glial cell types, such as surface glia, neuropil-associated glia and wrapping glia, as well as cortex glia (Fig. S1F), and is a top marker in that Fas cluster (Fig. S3B; Tables S3 and S4). One of the prominent features of the Fas cluster is the expression of cell adhesion proteins (Fas2, Fas3 and Ama), which is consistent with published findings underlying that cell–cell contact is a hallmark of glial cells (DeSalvo et al., 2014; Sasse et al., 2015). Thus, the Fas cluster does not appear to correspond to a specific cell type and therefore may represent a cell state.

Next, we performed Seurat analysis of a combined dataset of 9147 *repo*>*Ama*^{RNAi} cells and the 16,553 control cells to characterize glial cells differences between the knockdown and control brains. Cells of non-neuronal clusters were selected as above (Fig. 2B) and used to perform a supervised Seurat analysis. Reassuringly, the expression of *Ama* was strongly reduced in *repo*>*Ama*^{RNAi} cells (Fig. 2C), thus, indicating the efficiency of Ama depletion.

UMAP revealed several major differences in the presentation of *Ama*-depleted cells (Fig. 2D,E). First, there was a complete loss of the Fas cluster in *repo*>*Ama*^{RNAi} cells as it was represented exclusively by wild-type cells. Interestingly, this cluster displays the highest level of *Ama* expression (Fig. 2D,E). Second, *repo*>*Ama*^{RNAi} cells were missing in the SG cluster (Fig. 2D,E). Instead, *Ama*-depleted cells formed a distinct cluster that displayed the SG markers *Tret1-1*, *troll* and *CG3168* (Volkenhoff et al., 2015; Ariss et al., 2018) and was therefore labeled SG-like (SGL) (Fig. 2F; Fig. S4A). Third, the UMAP revealed a new Ama knockdown-specific cluster (ASC) (Fig. 2D,E) that expresses *repo* but none of other known glial cell markers (Fig. 2F; Tables S5 and S6). Instead *sprouty* (*sty*) is one of its top markers (Fig. S4B; Table S5). Finally, a hemocyte (HEMO) cluster was identified by the expression of blood cell markers such as *Hml* and *He* (Fig. S4B) (Goto et al., 2003; Kurucz et al., 2007), and this predominantly consisted of cells from the *repo*>*Ama*^{RNAi} brains (Fig. 2D,E). These results indicate that depletion of *Ama* affects multiple clusters at the single-cell level.

The BBB is disrupted upon Ama depletion

scRNA-seq profiling revealed that *Ama* is highly expressed in the Fas cell cluster and that this cluster is lost in *repo*>*Ama*^{RNAi} brains. To validate these results *in vivo*, we selected *Fas2*, a top marker of the Fas cluster, and examined its expression through immunofluorescence with anti-Fas2 antibody. Glial cells were labeled with membrane-targeted GFP using *repo*>*mCD8-GFP*. In the wild-type brain, Fas2 was observed in multiple glial cell types but with strongest expression in surface glia (Fig. 3A). This is consistent with published data showing that Fas2 is predominantly expressed in surface glia (DeSalvo et al., 2014). Notably, there was a striking reduction in Fas2 at the surface of the brain in SG cells of *repo*>*mCD8-GFP Ama*^{RNAi} brains (Fig. 3A). Such a defect in surface glia of *repo*>*Ama*^{RNAi} is particularly interesting given that SGL cells clustering distinctly from wild-type SG cells on the UMAP plot (Fig. 2D,E) suggesting that the gene expression profile of surface glial cells changes dramatically following *Ama* knockdown. We therefore decided to investigate the effect of Ama depletion in surface glia.

SG cells proliferate extensively during larval stages (Yildirim et al., 2019) in order to fully cover the rapidly increasing brain mass. This is essential for the maintenance of the BBB, a physical barrier that shields neurons from blood stream solutes and protects them from neurodegeneration (Yeh et al., 2018). The barrier is a vital component of the nervous system and it is damaged in multiple neurodegenerative diseases, such as Parkinson's and Alzheimer's diseases (Sweeney et al., 2018).

In order to determine whether Ama affects glial cell proliferation, the expression of cell cycle genes from the scRNA-seq dataset was examined. In comparison to wild-type controls, *repo*>*Ama*^{RNAi} glia strongly downregulate *PCNA*, *CycD*, *CycB*, *CycA* and *dpa* (Fig. 3B). Accordingly, there was a striking reduction of glial cells undergoing mitosis as revealed by immunostaining with an anti-PH3 antibody (Fig. 3C,D). These findings suggest that Ama plays a role in glial cell proliferation.

To examine the morphology of SG following *Ama* depletion, these cells were visualized with the C494 antibody, which labels SG membranes (Fig. S5A). In wild-type brains, C494 reveals a continues membrane layer that encompassed the brain. In contrast, surface glia membranes were discontinuous in *repo*>*Ama*^{RNAi} indicating that the brains were not completely covered by SG cells (Fig. 3E). This was confirmed with a different Gal4 driver, *moody-Gal4*, which is expressed in subperineurial glia (Fig. 3E). Discontinuity of SG membranes is a hallmark of a damaged BBB. To directly confirm this, *repo*>*Ama*^{RNAi} and *moody*>*Ama*^{RNAi} brains were incubated with a fluorescent dextran dye that only penetrates the brain when the BBB is broken (Bainton et al., 2005). Although no fluorescence signal was detected in control brains, both *repo*>*Ama*^{RNAi} and *moody*>*Ama*^{RNAi} brains displayed penetration of the fluorescent dye (Fig. 3F). Intriguingly, while analyzing the scRNA-seq dataset we noted an elevated number of hemocytes in the *repo*>*Ama*^{RNAi} condition relative to that in the control brain (Fig. 2D,E), which would be in agreement with a defective BBB. This was confirmed by staining with a pan hemocyte antibody (H2) (Kurucz et al., 2007), which showed a dramatic increase of infiltrating hemocytes in *repo*>*Ama*^{RNAi} brain lobes (Fig. 3G).

One of the consequences of disruption of BBB is the exposure of neurons to the high concentration of solutes in the hemolymph, which may cause neuronal degeneration and death. To determine whether Ama depletion in glia affects neurons, we examined the expression of apoptotic genes using scRNA-seq dataset.

Journal of Cell Science (2020) 133, jcs250837. doi:10.1242/jcs.250837

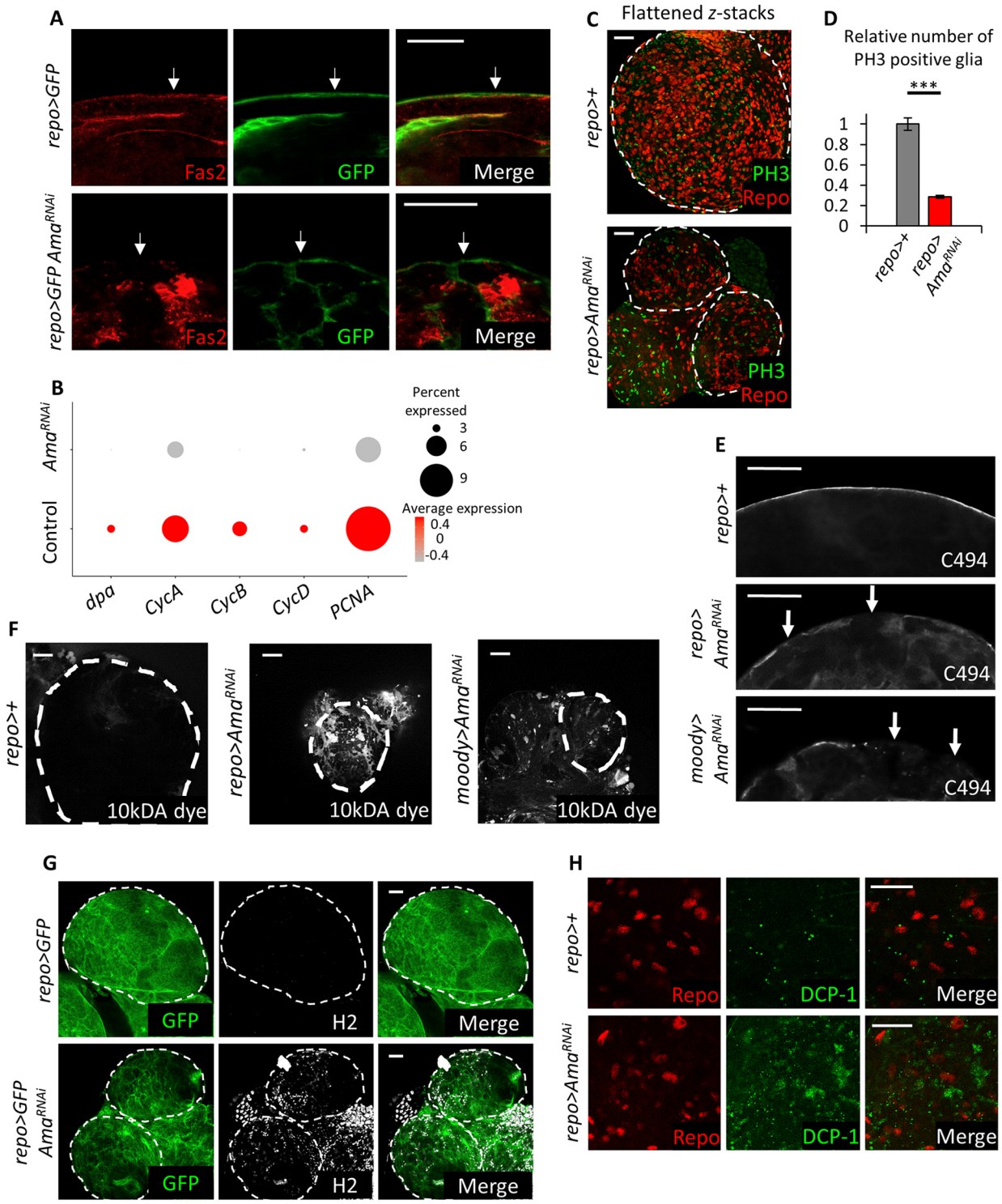

Fig. 3. Ama depletion decreases glial cell proliferation and disrupts the BBB. (A) Immunofluorescence images showing that there is a decrease in Fas2 in surface glia following Ama knockdown. Final genotype: *repo>mCD8GFP* (top panel) *repo>mCD8GFP Ama^{RNAi}* (bottom panel). White arrow points at surface glia. (B) Dot plot indicating a decrease in expression level of cell cycle genes *dpa*, *CycA*, *CycB*, *CycD*, and *PCNA* using scRNA-seq in *repo>+* and *repo>Ama^{RNAi}* glia. The red color gradient represents the average expression of the genes (average log fold change), whereas the size of the dot represents the percentage of cells expressing the genes. (C) Flattened *z*-stacks of *repo>+* and *repo>Ama^{RNAi}* brain immunofluorescence with REPO and PH3 showing that Ama knockdown decreases overall Repo and PH3 colocalization. (D) Quantification of Repo and PH3 colocalization in C reveals a significant reduction in mitotically active glia following Ama depletion. *Z*-stacks from *repo>+* (n=5) and *repo>Ama^{RNAi}* (n=6) brains were counted and normalized to the average count in *repo>+* (set at 1). Data represents the mean±s.e.m. after normalization. ***P<0.001 (Student's *t*-test; Table S9). (E) C494 immunofluorescence labeling SPG of third-instar larval brains showing discontinuous surface glia membranes following Ama knockdown. White arrows point to discontinuous membranes. (F) Brains labeled with 10 kDa dextran dye indicates that Ama knockdown increases dye penetration in the tissue, implying a damaged BBB. (G) Immunofluorescence using pan hemocyte H2 antibody shows a strong signal in the brain in *repo>Ama^{RNAi}*. (H) Cleaved DCP-1 immunofluorescence shows a neuronal apoptotic signal in *repo>Ama^{RNAi}*. Dashed outlines show brain regions. Scale bars: 20 µm.

Journal of Cell Science (2020) 133, jcs250837. doi:10.1242/jcs.250837

Interestingly, *hid*, a known pro-apoptotic gene in flies, is highly expressed in *repo>Ama*^{RNAi} cells but not in the wild-type cells of the neuronal cluster 6 (Fig. S5B–E). Accordingly, there was a significant level of neuronal death in *repo>Ama*^{RNAi} brains, as revealed by the staining with a cleaved DCP-1 antibody that labels the apoptotic cells (Fig. S5E).

We concluded that *Ama* has an essential function in glia because its glia-specific depletion severely impairs the BBB, leads to hemocyte infiltration into the brain and extensive neuronal cell death. The latter and severe proliferative defects of *Ama*-depleted glia may help to explain the small brain size in *repo>Ama*^{RNAi} animals.

Ama depletion reduces RTK signaling

The other major impact of Ama knockdown is the appearance of the ASC (Fig. 2D,F). Seurat analysis revealed that *sty*, a general RTK inhibitor (Hacohen et al., 1998), is an ASC top marker (Fig. S4B; Table S5). *sty* is highly upregulated in *Ama*-depleted glia cells, while the expression of a downstream effector and a read-out of RTK signaling in glia *pointed* (*pnt*) (O'Neill et al., 1994) is reduced (Fig. 4A). Interestingly, RTK signaling through FGFR (Avet-Rochex et al., 2012) and PDGFR (Read, 2018) has been shown to be important for glial cell proliferation in the third-instar brain as well as for glial migration (Franzdóttir et al., 2009). Since Ama-deficient glia proliferate poorly and fail to migrate from brain to the eye disc, we investigated RTK signaling in the *repo>Ama*^{RNAi} brain.

We began by examining the Sty expression in surface glia cells of *repo>Ama*^{RNAi} brains by immunofluorescence using a Sty antibody that has been previously validated (Hacohen et al., 1998). In the control, Sty is present at a low level uniformly throughout the confocal plane. In *Ama*-depleted glia, Sty was markedly elevated especially at plasma and nuclear membranes, and this result was confirmed with two different *UAS-Ama*^{RNAi} lines (Fig. 4B,C; Fig. S6A). Conversely, Sty staining was moderately reduced when Ama was overexpressed using a *repo-Gal4* driver (Fig. 4B,C). To determine whether changes in Sty levels in *Ama* depleted glia are consequential, we examined the phospho-ERK (P-ERK) staining, a commonly used marker of RTK signaling, in surface glia. Strikingly, the P-ERK signal was largely lost in *repo>Ama*^{RNAi} while overexpression of Ama resulted in a modest increase in P-ERK (Fig. 4D,E). Another readout of RTK signaling, Pointed (PntP1), was strongly reduced in *Ama*-depleted glia and slightly elevated in *repo>Ama* (Fig. 4F), which is in agreement with scRNA-seq data (Fig. 4A).

Since Ama is found at the membrane and is also secreted (Fremion et al., 2000), we asked whether it could exert a non-cell-autonomous effect on P-ERK. Clones of glia cells overexpressing Ama were generated by heat shock in a *hs-FLP Act≫Ama GFP* line, stained with P-ERK and distinguished by GFP. Notably, an elevated P-ERK signal was observed within the clone of cells expressing Ama (GFP positive) as well as in cells adjacent to the clonal boundary (Fig. 4G). This suggests that Ama can affect RTK signaling in non-cell-autonomous manner. Additionally, ectopic expression of Ama in the posterior of the eye disc resulted in elevated P-ERK and a rough eye phenotype (Fig. S7A–C), while clonal analysis demonstrates a non-cell-autonomous effect (Fig. S7D). We also note that an increase in Sty levels occur in PG and SPG even when Ama is depleted using an SPG driver (Fig. S6A). This also suggests that the effect of Ama on Sty can occur in a non-cell-autonomous manner, which may, in turn, explain the non-cell-autonomous impact of Ama on RTK activity described above.

These findings suggest that Ama affects RTK in different cell types and can act in a non-cell-autonomous manner. This is consistent with previous biochemical studies of Ama showing that it is present at the plasma membrane and is also secreted (Fremion et al., 2000).

Ama affects RTK signaling through Sty

As described above, *repo>Ama*^{RNAi} animals have reduced glial cell proliferation, a small brain size and defects in glial migration. Previous studies highlight the importance of RTK signaling in proliferation and migration of glial cells (Avet-Rochex et al., 2012; Read, 2018; Franzdóttir et al., 2009). Our results show that a major consequence of Ama knockdown is upregulation of Sty, a negative regulator of the RTK pathway, and reduced RTK signaling. These observations suggest a simple model where a high level of Sty in *Ama* depleted cells lowers RTK signaling in these cells and may account for the *Ama* phenotype.

This model was tested in two ways. First, we asked whether upregulation of Sty is an important event in *Ama*-depleted glia. This was determined by a genetic test in which Sty was downregulated by RNAi in glial cells, after which brains of *repo>sty*^{RNAi}*Ama*^{RNAi} and *repo>Ama*^{RNAi} were compared. The efficiency of *sty* RNAi was confirmed by staining with the Sty antibody, and showed that Sty was no longer upregulated in *repo>sty*^{RNAi}*Ama*^{RNAi} (Fig. S8A). Downregulation of Sty partially rescued the small brain size of *repo>Ama*^{RNAi} as the *repo>sty*^{RNAi} *Ama*^{RNAi} brains were larger in size than in *repo>Ama*^{RNAi} brains (Fig. 5A). Accordingly, cell counting showed a significant increase in the number of glial cells in *repo>sty*^{RNAi} *Ama*^{RNAi} compared to the number in *repo>Ama*^{RNAi} (Fig. 5B). However, Sty depletion was insufficient to rescue the discontinuous SPG membranes and neuronal cell death, as there was no significant difference in the C494 and DCP-1 staining, respectively, between *repo>Ama*^{RNAi} and *repo>sty*^{RNAi} *Ama*^{RNAi} conditions (Fig. S8B,C). However, we cannot completely exclude the possibility that Sty is involved in the effect of Ama on the BBB.

As another test of the model, we asked whether Erk [also known as Rolled (Rl) in flies], which is downstream of Sty and therefore insensitive to Sty upregulation, rescues the phenotype of Ama depletion. To do this, a constitutively active Erk transgene (*UAS-rl*^{sem}) was overexpressed in *Ama*-depleted glial cells. As shown in Fig. 5A, brains of *repo>rl*^{sem} *Ama*^{RNAi} animals were significantly larger than those of *repo>Ama*^{RNAi} and there was a significant increase in glial cell number relative to *repo>Ama*^{RNAi} (Fig. 5B). Interestingly, glial migration on the eye disc was partially rescued in *repo>rl*^{sem} *Ama*^{RNAi} (Fig. 5C), further underscoring the importance of RTK and ERK in this process.

From these results, we conclude that the phenotype of glial-specific Ama knockdown is, at least partially, caused by reduced RTK signaling given that elevating RTK signaling through expression of activated ERK largely rescues glial cell migration and the small brain size in *repo>Ama*^{RNAi}. Our results suggest that Ama is upstream of ERK and acts through Sty to alter RTK signaling. Thus, upregulation of Sty is functionally important in Ama-depleted cells.

Ama knockdown suppresses neoplasia in a *Drosophila* glioma model

One of the best cancer models developed in *Drosophila* is a glioma model in which co-activation of the EGFR-Ras and PI3K pathways faithfully recapitulates many hallmarks of human glioma (Furnari et al., 2007). In the glioma fly model, co-expression of *dEGFR*$^{\lambda}$ and *dp110*^{CAAX} transgenes in glial cells

Journal of Cell Science (2020) 133, jcs250837. doi:10.1242/jcs.250837

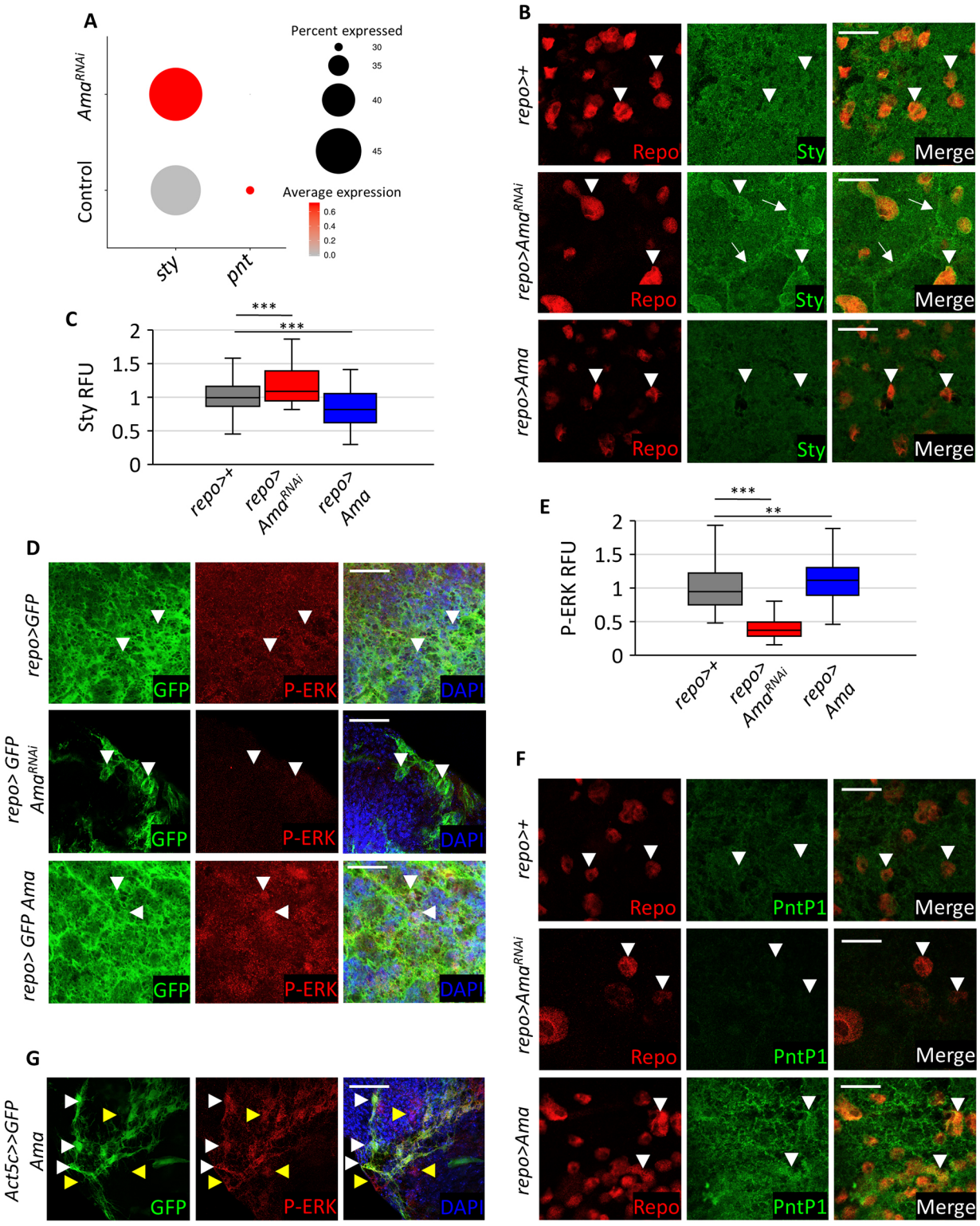

Fig. 4. See next page for legend.

gives rise to highly proliferative, transplantable and invasive neoplastic tumor-like growth (Read et al., 2009). Since Ama is important in regulation of normal RTK signaling during development, we asked whether the role of Ama is conserved in the oncogenic context of the glioma model.

As expected, glial-specific expression of $dEGFR^{\lambda}$ and $dp110^{CAAX}$ resulted in the activation of EGFR-Ras pathway, which was visualized by a dramatic increase in the P-ERK and PntP1 staining relative to the control (Fig. 6A,B) (Read et al., 2009). This led to excessive glia proliferation and enlargement of the brain (Fig. 6C) (Read et al., 2009). Remarkably, concomitant depletion of Ama blocked hyperactivation of the pathway as the levels of P-ERK and PntP1 were reduced below the wild-type control (Fig. 6A,B). Accordingly, Ama depletion reduced the abnormally large brain

Journal of Cell Science (2020) 133, jcs250837. doi:10.1242/jcs.250837

Fig. 4. Ama knockdown decreases RTK signaling. (A) Dot plot showing an increase in *sty* and a decrease in *pnt* as determined through scRNA-seq in *repo>Ama*^{RNAi} relative to *repo*>+. The red color gradient represents the average expression of *sty* or *pnt* (average log fold change), whereas the size of the dot represents the percentage of cells expressing sty or *pnt*. (B) Sty immunofluorescence in surface glia shows an increase in Sty especially at the membrane in *repo>Ama*^{RNAi} and a modest decrease in basal Sty in *repo>Ama*. White arrowheads point to Repo-positive glial cells, whereas white arrows point to SPG membranes. (C) Box plot displaying the Sty relative fluorescence units (RFU) measured in surface glia in each *repo*>+ (*n*=70 nuclei, across 5 brains), *repo>Ama*^{RNAi} (*n*=84 nuclei, across 8 brains), and *repo>Ama* (*n*=162 nuclei, across 9 brains). The RFUs were normalized to the average Sty RFU value in 70 *repo*>+ nuclei. The line in the center of the box represents the median. The lower and upper box limits are the first and third quartiles, respectively. The Tukey whiskers extend to show the minimum and maximum values outside the first and third quartiles. ***P<0.001 (Student's *t*-test) to compare each genotype to *repo*>+ (Table S10). (D) P-ERK immunofluorescence in surface glia shows a decrease in P-ERK signal in *repo>Ama*^{RNAi} and a modest increase in P-ERK in *repo>Ama*. White arrowheads point at glia nuclei. Final genotypes: *repo>mCD8GFP* (top panel), *repo>mCD8GFP Ama* (middle panel), *repo>mCD8GFP Ama*^{RNAi} (bottom panel). (E) Box plot displaying the P-ERK RFU measured in surface glia in each *repo*>+ (*n*=171 nuclei, across 17 brains), *repo>Ama*^{RNAi} (*n*=173 nuclei, across 15 brains), and *repo>Ama* (*n*=118 nuclei, across 15 brains). The RFUs were normalized to the average *P*-ERK RFU value in 171 *repo*>+ nuclei. The line in the center of the box represents the median. The lower and upper box limits are the first and third quartiles, respectively. The Tukey whiskers extend to show the minimum and maximum values outside the first and third quartiles. **P<0.01, ***P<0.001 (Student's *t*-test) to compare each genotype to *repo*>+ (Table S11). (F) Immunofluorescence images in SG using PntP1 antibodies reveals that there is a decrease in signal in *repo>Ama*^{RNAi} and a modest increase in PntP1 in *repo>Ama*. White arrowheads point at Repo-positive glia nuclei. Final genotypes: *repo>mCD8GFP* (top panel), *repo>mCD8GFP Ama* (middle panel), *repo>mCD8GFP Ama*^{RNAi} (bottom panel). (G) P-ERK immunofluorescence in a clone of cells using FLP-Out to overexpress Ama. GFP labels PG cells in the clone on the surface of the brain that over express Ama. White arrowheads point at cell autonomous increase of P-ERK. Yellow arrowheads point at cell non-autonomous increase of P-ERK. Scale bars: 20 µm.

size of *repo>dEGFR*$^{\lambda}$ *dp110*^{CAAX} (Fig. 6C). Since upregulation of Sty is a key event of Ama downregulation, we compared Sty expression between *repo>dEGFR*$^{\lambda}$ *dp110*^{CAAX} and *repo>dEGFR*$^{\lambda}$ *dp110*^{CAAX} *Ama*. In *repo>dEGFR*$^{\lambda}$ *dp110*^{CAAX} brains, Sty was uniformly upregulated throughout the glial plane (Fig. 6D). This is expected as Sty was shown to be directly regulated by EGFR signaling (Butchar et al., 2012) and fine-tunes RTK signaling (Rubin et al., 2003). Strikingly, in *repo>dEGFR*$^{\lambda}$ *dp110*^{CAAX} *Ama*^{RNAi} glial cells, Sty was upregulated to a much higher level that was especially evident at the nuclear membrane (Fig. 6D). Thus, Ama depletion results in increase of Sty, reduces RTK activation caused by activated EGFR and blocks neoplasia in a glioma fly model.

Knockdown of the Ama ortholog LSAMP increases SPROUTY2 levels in human glioblastoma cell lines

Ama has several human orthologs that belong to the IgLON immunoglobulin cell adhesion family (https://flybase.org/; Thurmond et al., 2019), with one member of this family LSAMP showing the highest sequence similarity. Interestingly, IgLONs family members are expressed in astrocyte glia and have been shown to promote astrocyte proliferation through FGF signaling (Sugimoto et al., 2012). The experiments described above suggest that upregulation of Sty is the major consequence of Ama depletion in glia during normal development and in the glioma model. Therefore, we asked whether the relationship between Ama and Sty is conserved in human cells.

To address this question, we selected two glioblastoma cell lines, U251 and T98G, and examined the expression of SPROUTY2 (SPRY2) following LSAMP knockdown by western blotting. Endogenous LSAMP was detected in U251 and T98G glioblastoma cell lines by western blotting (Fig. 7A,B). U251 cells expressing *LSAMP* shRNA were generated using a lentiviral construct, and western blotting confirmed that LSAMP was successfully knocked down by the *LSAMPsh* (Fig. 7A). A doxycycline (Dox)-inducible knockdown system was generated in the T98G cell line, since conventional lentiviral shRNA resulted in reduced cell viability. A dose-dependent decrease in LSAMP was observed with increasing concentration of Dox (Fig. 7B). Having established the efficiency of LSAMP knockdown, we examined SPRY2 levels. As shown in Fig. 7A,B, in both U251 and T98G cell lines, *LSAMPsh* expression led to an increase in SPRY2 expression, as revealed by western blotting.

To explore the relationship between LSAMP and SPRY2 in human glioblastoma, we analyzed the publicly available glioblastoma multiforme (GBM) TCGA PanCancer Atlas database (cBioportal.org). We found a significant inverse correlation in mRNA levels between *LSAMP* and *SPRY2* (Fig. 7C). GBM patients with *EGFR* mutations and amplifications were selected to perform Kaplan–Meier survival analyses based on *LSAMP* expression. The results revealed a significant decrease in survival in patients with high expression of *LSAMP* (Fig. 7D,E). These findings suggest that the relationship between Ama and Sty is conserved in human glioblastoma cell lines.

DISCUSSION

The RTK signaling pathway is critical in a plethora of glial cell functions, such as migration, differentiation, proliferation, neurodegeneration and locomotion (Yildirim et al., 2019; Ray et al., 2017). Here, we identify Ama as a regulator of RTK signaling in glial cells and uncover an essential function of Ama in the maintenance of the BBB. Our study underscores the power of scRNA-seq profiling to explore a knockdown phenotype and led to the identification of Sty as a major Ama target during regulation of RTK signaling.

Profiling cells by scRNA-seq identified distinct changes in gene expression profiles across multiple glial cell types in *Ama*-depleted brain that otherwise would have not been possible using conventional approaches. First, we find that Ama depletion affects gene expression in surface glia, which in turn leads to a disruption in the BBB. Second, the increase in hemocyte numbers in *repo>Ama*^{RNAi} scRNA-seq dataset enabled the discovery of infiltrating blood cells in *Ama*-depleted brains. Third, the increase in Sty and decrease in PntP1 levels following Ama knockdown in glia guided us to explore the impact of Ama in RTK signaling.

scRNA-seq identifies and clusters cells based on similarity in gene expression profile to uncover the cellular heterogeneity in a tissue. In this study, scRNA-seq of the normal fly brains identified all the glial cell types in addition to a Fas cluster that appeared to encompass multiple glial cell types. This cell cluster displayed high expression levels of cell adhesion proteins, which is a hallmark of glial cells (DeSalvo et al., 2014; Sasse et al., 2015), while also supporting the observation that scRNA-seq not only clusters cells by type but also by similar biological features (Ariss et al., 2018). This underlies the robustness of scRNA-seq, since it uncovers complex cellular dynamics related to certain stimuli and continuous temporal differentiation processes (Liu and Trapnell, 2016), as well as the spatial arrangement of cells (Wagner et al., 2016). Notably, the cellular perturbations in clustering that we observed following

Journal of Cell Science (2020) 133, jcs250837. doi:10.1242/jcs.250837

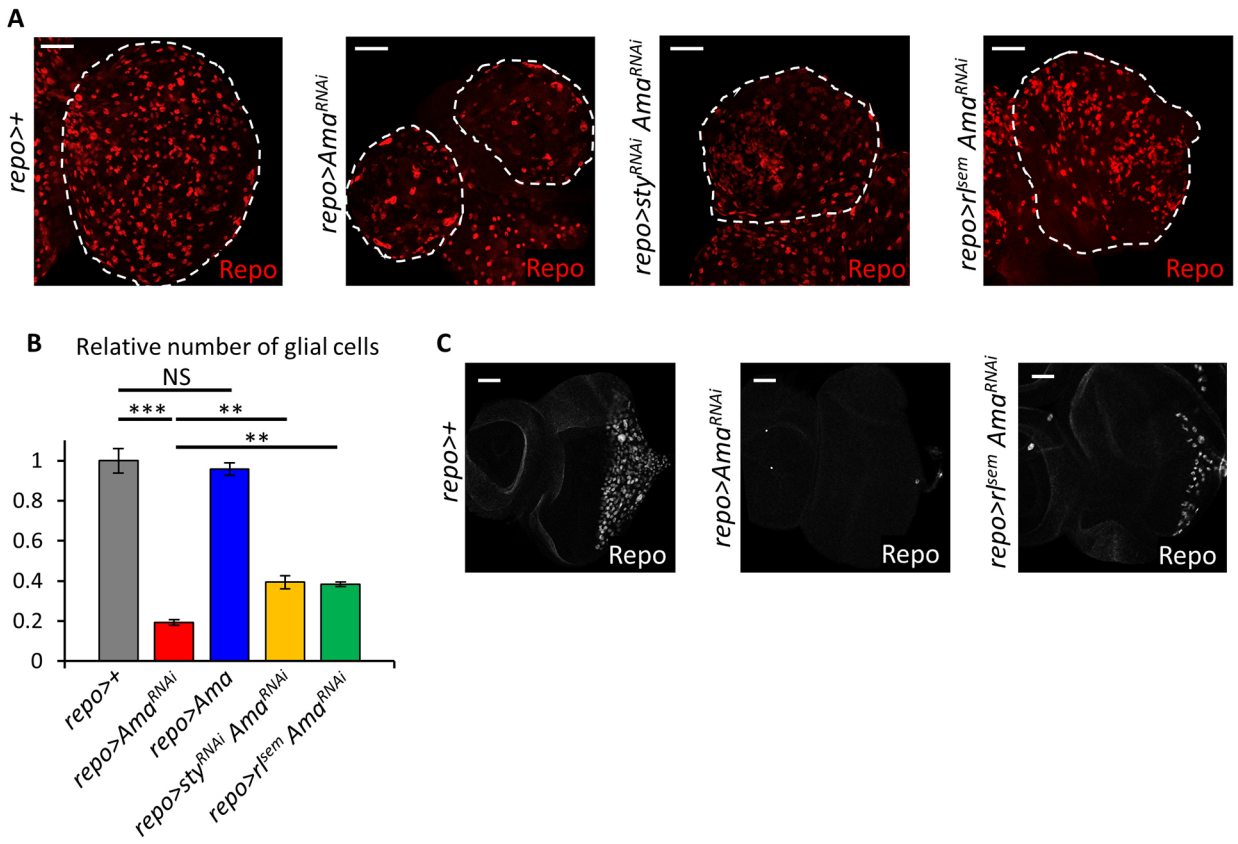

Fig. 5. Sty knockdown largely rescues the phenotype of Ama depletion. (A) Repo immunofluorescence of third-instar larval brains show a partial increase in size in *repo>sty*^{RNAi} *Ama*^{RNAi}, and *repo>rl*^{sem} *Ama*^{RNAi} relative to that in *repo>Ama*^{RNAi}. Dashed outlines show brain regions. (B) Quantification of Repo in brains in A reveal that *sty* knockdown or overexpressing activated ERK in *Ama*-depleted brains partially rescues the number of glia *repo>Ama*^{RNAi}. *Z*-stacks from *repo>+* (*n*=4), *repo>Ama*^{RNAi} (*n*=4), *repo>Ama* (*n*=3), *repo>Ama*^{RNAi} (*n*=4), *repo>sty*^{RNAi} *Ama*^{RNAi} (*n*=4), *repo>rl*^{sem} *Ama*^{RNAi} (*n*=4) brains were counted and values normalized to the average count in *repo>+* (set at 1). Data represents the mean±s.e.m. after normalization. ***P*<0.01; ****P*<0.001; NS, not significant (Student's *t*-test) to compare each genotype to *repo>+* (Table S12). (C) Repo immunofluorescence of eye discs indicates that overexpression of activated ERK in *Ama*-depleted brains partially rescues glial cell migration in *repo>Ama*^{RNAi} eye discs. Scale bars: 20 µm.

Ama depletion were validated experimentally by genetic analysis, immunofluorescence and other assays. This type of single-cell data validation is essential as it addresses the concern of a batch effect between scRNA-seq samples (Haghverdi et al., 2018). Thus, our work highlights the power of scRNA-seq to profile a knockdown or mutant phenotype.

Our results revealed that Ama is critical for maintaining the BBB, as its depletion results in discontinuous SG membranes, suggesting a lack of tight junctions or organization that leads to disruption of the barrier (Babatz et al., 2018). This in turn exposes the larval brains to the high potassium content of the hemolymph, which damages neurons (Yildirim et al., 2019). Ama knockdown decreases overall glial cell proliferation, which can affect SG cells and the BBB in two additional ways. First, lack of proliferation in PG cells can potentially affect the secretion of metabolites, which is important to prevent neurodegeneration (Volkenhoff et al., 2015). Second, Ama depletion can alter SPG growth by reducing endoreplication and endomitosis, as evident by reduced expression of cell cycle genes in *repo>Ama*^{RNAi}, and, therefore, hinder the ability of SPG to accommodate the growing brain during late larval stages (Unhavaithaya and Orr-Weaver, 2012).

The conventional way to determine the intactness of the BBB function is by labeling brains with a fluorescent dextran dye. If the barrier is permissible to large molecules, such as the dye, then the BBB is considered to be broken. Here, we present an alternative approach to monitor a disruption in the BBB by measuring the increase in infiltrating hemocytes in larval brains both by scRNA-seq and through staining with a hemocyte-specific antibody. Although SG protect neurons from the hemolymph (Yeh et al., 2018), penetration of hemocytes into the brain through the damaged BBB has not been previously reported. Whether infiltrating hemocytes have a role in inflicting the damage in the brain is unknown but raises the possibility that they might have a function in that context.

Ama and Lachesin are part of the IgLON family, with Lachesin also shown to be required for the BBB maintenance (Strigini et al., 2006). Since IgLONs are also expressed in the BBB in mammals, this suggests that the immunoglobin superfamily may indeed also have an evolutionarily conserved BBB function in humans (Kubick et al., 2018). These findings highlight an important role of IgLONs in neurodegenerative diseases that result in BBB breakdown (Sweeney et al., 2018).

Through scRNA-seq and measuring P-ERK and PntP1 levels, we found a drastic reduction in the level of RTK signaling in *Ama*-depleted brains. We suggest that Ama regulates the RTK pathway since its depletion increases Sty levels, a general inhibitor of the pathway, and, conversely, overexpression of Ama has an opposite effect. Sty in *repo>Ama*^{RNAi} brains predominantly localizes to the nuclear and plasma membranes. Intriguingly, in mammalian cells, SPRY2 localization to the membrane has been shown to be crucial for its phosphorylation and inhibitory effect (Hanafusa et al., 2002).

Journal of Cell Science (2020) 133, jcs250837. doi:10.1242/jcs.250837

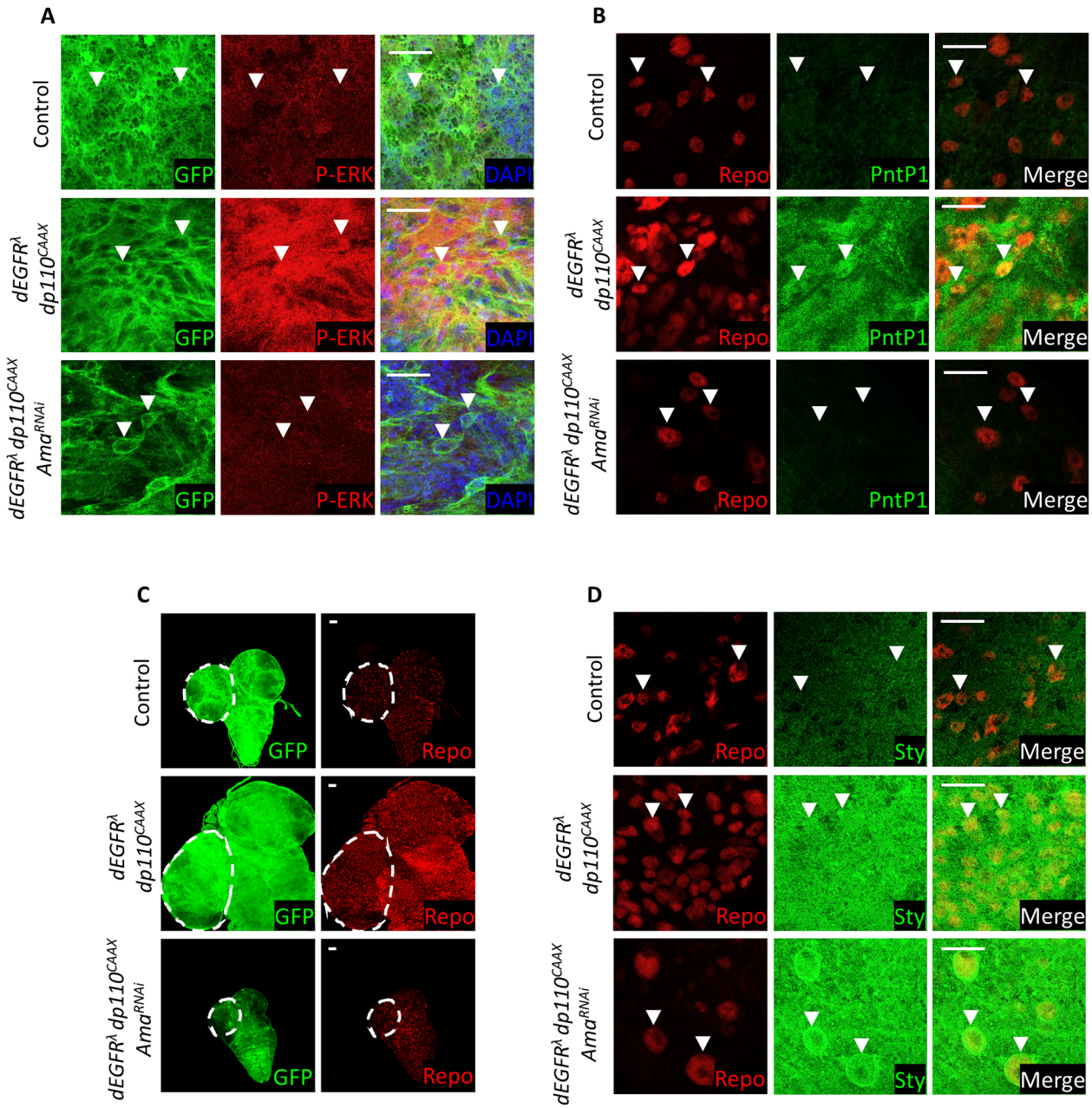

Fig. 6. Ama depletion suppresses neoplastic growth in the *Drosophila* glioma model. (A) P-ERK immunofluorescence in surface glia reveals that knockdown of Ama in the *Drosophila* glioma model causes a striking decrease in P-ERK. White arrowheads point at glial cells. (B) PntP1 immunofluorescence in surface glia indicates that there is a drastic decrease in PntP1 following Ama depletion in the *Drosophila* glioma model. White arrowheads point at Repo-positive glial cells. (C) Repo immunofluorescence in surface glia shows that Ama depletion in a *Drosophila* glioma model drastically decreases the brain size and number of glia. GFP labels glial cell membranes. Dashed outlines show brain regions. (D) Immunofluorescence reveals that there is an increase in Sty levels following Ama knockdown in the *Drosophila* glioma model in surface glia. White arrowheads point at Repo-positive glial cells. Scale bars: 20 µm. Final genotypes in A–D: *repo>mCD8GFP* (top panel), *repo>dEGFR$^{\lambda}$ dp110^{CAAX} mCD8GFP* (middle panel), *repo>dEGFR$^{\lambda}$ dp110^{CAAX} mCD8GFP Ama^{RNAi}* (bottom panel).

Our results therefore suggest that, while depletion of Ama increases Sty levels, there might additionally be an effect in the cellular localization or post-translational modification of Sty (Jarvis et al., 2006). Genetic experiments indicate that Sty is the key target of Ama and that activated ERK can partially rescue the *repo>Ama^{RNAi}* phenotype, whereas activated EGFR in the glioma fly model cannot. These epistatic interactions support the model that Ama, acts through Sty, and is downstream of EGFR but upstream of ERK in the RTK signaling pathway (Fig. 8).

Although knockdown of Sty in Ama-depleted brains partially rescues the glial cell numbers and brain size, it fails to suppress the neuronal apoptosis in *repo>Ama^{RNAi}* brains. Since Ama can act non-cell-autonomously, we cannot exclude the possibility that Ama might also affect neurons non-cell-autonomously and, therefore, the expression of Sty in glial cells fails to rescue neurons. This is noteworthy since LSAMP, the human counterpart of Ama, was reported to control neurite growth (Akeel et al., 2011). The precise mechanism of how Ama affects Sty is unknown and requires further investigation. However, SPRY2 and EGFR in human cell lines have been shown to compete with c-Cbl (a ubiquitin ligase) binding. In this context, the ubiquitin ligase attenuates the inhibitory effect of SPRY2 and vice versa (Rubin et al., 2003). Since Ama and Sty

Journal of Cell Science (2020) 133, jcs250837. doi:10.1242/jcs.250837

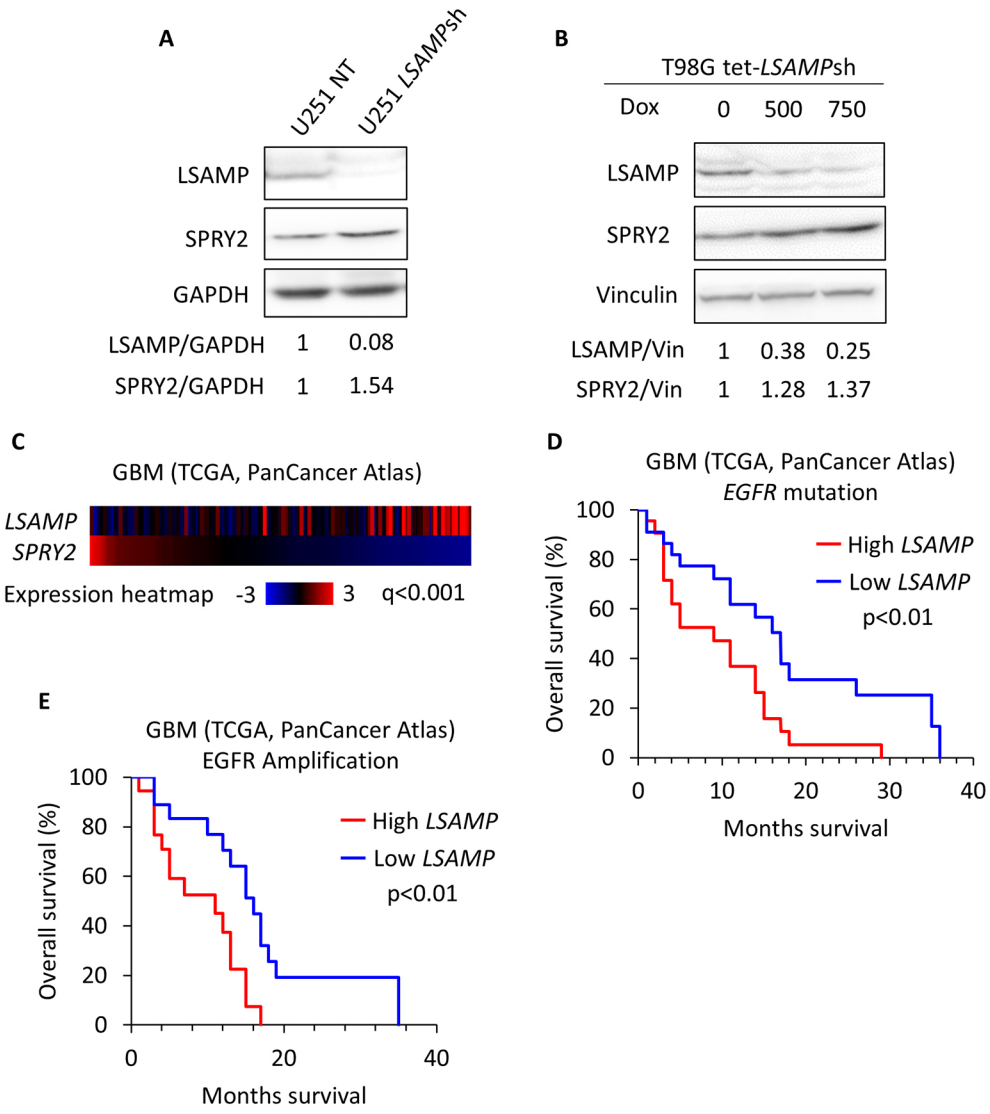

Fig. 7. The relationship between Ama and Sprouty is conserved in human glioblastoma cell lines. (A) Immunoblot showing LSAMP, SPRY2 and GAPDH levels in U251 cells stably expressing non-targeting shRNA (NT) or *LSAMP* shRNA (*LSAMP*sh). Knockdown of LSAMP increases SPRY2, with relative densitometry levels for each target labeled below. (B) Immunoblot showing LSAMP, SPRY2 and vinculin levels in T98G cells expressing a doxycycline-inducible shRNA. Cells were treated for 3 days with the corresponding amounts of doxycycline (ng/ml in 0.15% DMSO) before harvesting. Dose-dependent knockdown of LSAMP gradually increases SPRY2. Relative densitometry levels for each target are labeled below. Results in A and B are representative of three independent experiments. (C) Heatmap displaying mRNA expression *z*-score (RNA Seq V2 RSEM) of *LSAMP* and *SPRY2* in each row in GBM human patients (TCGA PanCancer Atlas) showing a significant inverse correlation between those genes. Each column represents a tumor tissue sample. The q-value was generated from a two-sample *t*-test. (D) Kaplan–Meier plot revealing that GBM patients (TCGA PanCancer Atlas) with EGFR mutations have a significant decrease in survivability with high levels of *LSAMP* mRNA. The *P*-value was generated from a logrank test. (E) Kaplan–Meier plot of GBM patients with EGFR amplifications reveals that patients with high *LSAMP* mRNA have a significant decrease in survivability. The *P*-value was generated using a logrank test.

localize to cell membranes, one possible explanation is that they may interact with each other, whereby loss of Ama releases Sty to bind to RTK receptors and promotes inhibition of the signaling pathway.

Finally, we show that the role of Ama in controlling Sty levels is conserved in human glioblastoma (GBM) cell lines. Additionally, GBM patients with EGFR mutations display a significant increase in survival when they have low expression levels of LSAMP, suggesting a potential role for the IgLON family member in this cancer. Previous work has shown that LSAMP either promotes growth or acts as a tumor suppressor (Kresse et al., 2009). Intriguingly, SPRY2 inhibits or activates RTK signaling based on the context and cell type and also acts either as an oncogene or tumor suppressor (Masoumi-Moghaddam et al., 2014). Our results suggest a potential connection between LSAMP and SPRY2 that may help to explain the role of LSAMP in tumorigenesis and, thus, point to *LSAMP* as a potential therapeutic target.

MATERIALS AND METHODS

Fly stocks

Drosophila stocks and crosses were kept at 25°C using standard cornmeal agar medium unless mentioned otherwise. Stocks were obtained from the Bloomington Drosophila Stock Center (BDSC) the Kyoto Drosophila Genetic Resource Center (DGRC), and the Vienna Drosophila Resource Center (VDRC).

The stocks used were: (1) *w[1118]; P{w[+m*]=GAL4}repo/TM3, Sb[1]* (BDSC *P{GAL4}repo*); (2) *y[1] sc[*] v[1] sev[21]; P{y[+t7.7] v[+t1.8]=TRiP.HMS00297}attP2* (BDSC *HMS00297*, *UAS-Ama^{RNAi}*); (3) *y[1] v[1]; P{y[+t7.7] v[+t1.8]=UAS-GFP.VALIUM10}attP2* (BDSC); (4) *w[*]; P{y[+t7.7] w[+mC]=10XUAS-IVS-mCD8::GFP}attP2* (BDSC); (5) *y[*] w[*]; P{w[+mW.hs]=GawB}Ama[NP1297] / TM6, P{w[-]=UAS-lacZ.UW23-1}UW23-1* (Kyoto DGRC); (6) *moody-Gal4* (gift from Vicki Losick, Biology Department, Boston College, USA); (7) *UAS-dEGFR$^{\lambda}$, UAS-dp110^{CAAX}; repo-Gal4, UAS-mCD8-GFP/TM6C, Tb, tub-Gal80* (gift from Renee Read, Department of Pharmacology and Chemical Biology, Emory University School of Medicine, USA); (8) *repo-Gal4, UAS-mCD8-GFP/TM6C, Tb* (gift from Renee Read); (9) *UAS-sty^{RNAi}* (VDRC shRNA330208); (10) *y[1] w[*]; P{w[+mC]=UAS-rl[Sem].S}2* (BDSC); (11) *w[1118]; P{y[+t7.7] w[+mC]=GMR57E08-GAL4}attP2* (BDSC); (12) *y[1] w[*]; P{y[+t7.7] w[+mC]=E(spl)mdelta-HLH-GFP.FPTB}attP40* (BDSC); (13) *hs-FLP; act5c-FRT-stop-FRT-Gal4, UAS-GFP* (gift from Teresa Orenic, Biological Sciences Department, University of Illinois at Chicago, USA); (14) *UAS-Ama^{RNAi}* (VDRC GD22945).

The *moody>Ama^{RNAi}* (VDRC GD22945) cross was performed at 25°C for 2 days then the vial was transferred to 30°C for the rest of development.

All the Ama knockdown experiments were performed using BDSC HMS00297 unless the VDRC GD22945 UAS-Ama^{RNAi} line is mentioned in figure and figure legend.

Journal of Cell Science (2020) 133, jcs250837. doi:10.1242/jcs.250837

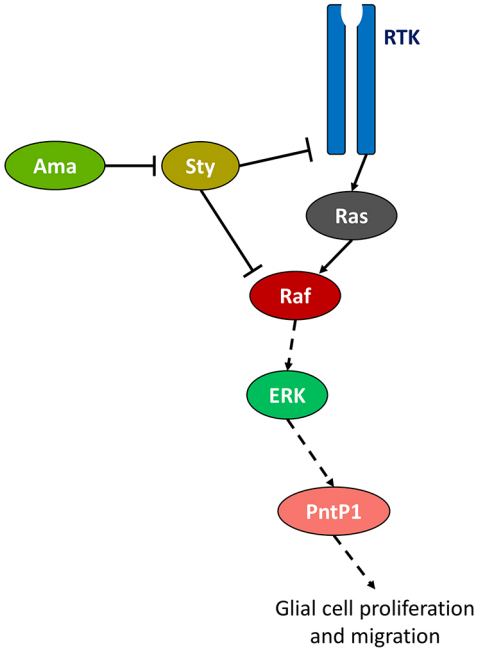

Fig. 8. Ama affects RTK signaling. Illustration of the molecular mechanism of Ama acting through Sty to inhibit RTK signaling.

Ama transgene

A UAS-Ama C-terminal FLAG-HA tagged clone UFO01101 having a *white* gene selectable marker and an *attB* site was used from the Universal Proteomics Resource and part of the Berkeley Drosophila Genome Project (BDGP) (https://www.fruitfly.org/EST/proteomics.shtml). This clone was received from the Drosophila Genomics Resource Center (DGRC) (https://dgrc.bio.indiana.edu/Home) stock number 1621050.

The PhiC31 transformation services in BestGene (http://www.thebestgene.com/) were performed on the *y[1] w[1118]; PBac{y[+]-attP-9A}VK00023* line (BDSC 9741) with an estimated CytoSite 70A2 (chromosome 3) using the UAS-Ama construct above.

Fluorescence *in situ* hybridization

A total of 38 RNA probes labeled with Quasar 670 fluorophores were generated with the Stellaris custom probe designer v4.2 that target the Ama-RA coding sequence (oligonucleotide length=18; min. spacing length=2; masking level=5) (https://biosearchassets.blob.core.windows.net/assets/bti_custom_stellaris_drosophila_protocol.pdf).

Third-instar larval brains were dissected and the Stellaris imaginal disc fluorescence *in situ* hybridization protocol was followed (https://biosearchassets.blob.core.windows.net/assets/bti_custom_stellaris_drosophila_protocol.pdf). Samples were imaged using a Zeiss Confocal microscope.

Immunofluorescence

Third-instar larval brains were dissected in 1× PBS then fixed for 30 min in 4% formaldehyde in 1× PBS. The brains were permeabilized and washed twice with 0.3% PBST (1× PBS and 0.3% Triton X-100) for 10 min. Primary antibodies were incubated overnight in 10% normal donkey serum (NDS; Jackson Immunoresearch). The samples were washed three times on the second day with 0.1% PBST (1× PBS and 0.1% Triton X-100) and incubated with the fluorescently labeled secondary antibody in 10% NDS for 1 h. Brains were then washed five times with 0.1% PBST and mounted on a glass slide using FluorSave (EMD Millipore).

Wandering third-instar larval eye discs were dissected in 1× PBS and fixed in 4% formaldehyde in 1× PBS for 15 min, permeabilized in 0.3% PBST two times for 10 min and then incubated with antibodies overnight at 4°C in 1× PBS plus 10% NDS and 0.1% Triton X-100 blocking serum. The following day, samples were washed in 0.1% PBST three times for 5 min. Samples were then incubated with appropriate fluorescently labeled secondary antibodies (Jackson Immunoresearch) for 1 h in 1× PBS plus 10% NDS and 0.1% Triton X-100 followed by 4′,6-diamidino-2-phenylindole (DAPI) for 5 min. Finally, samples were washed five times for 5 min then mounted in FluorSave (EMD Millipore) on glass slides. All steps were carried out at room temperature and with gentle rocking, unless specified otherwise. Whenever fluorescence images have been compared, they were obtained with the same acquisition and display settings. The slides were imaged using Zeiss Confocal microscope.

Primary antibodies were used: anti-Repo: DSHB 8D13 (1:50), anti-cleaved *Drosophila* Dcp-1 (Cell Signaling Asp216; 1:500), anti-GFP (FITC) (Abcam ab6662; 1:1000), anti-P-ERK (Sigma M8159; 1:200), anti-Sty-C-terminal (a gift from Mark Krasnow, Biochemistry Department, Stanford University, USA; 1:900), anti-P-Glycoprotein, C494 (recommended by Roland Bainton, Department of Anesthesia and Perioperative Care, University of California, San Francisco, USA; ThermoFisher Scientific MA1-26529 1:100), anti-Fas2 (DSHB 1D4; 1:50), anti-PH3 (Millipore Sigma 06-570, 1:1000), 24B10 antibody (DSHB; 1:100), anti-PntP1 (gift from James Skeath, Department of Genetics, Washington University, USA; 1:200), H2 antibody (gift from István Ando, Institute of Genetics, Hungarian Academy of Sciences, Hungary; 1:100).

Heat-shock treatment

To generate third-instar larvae with clones of cells that overexpress Ama, heat shock was induced 72 h after egg deposition at 37°C for 1 h then embryos were transferred to 25°C. Third-instar larvae were collected around 55 h after heat-shock for immunostaining.

Dextran labeling

Larval brains were dissected and rinsed twice with 1× PBS then incubated for 10 to 15 min in 2.5 mM of Tetramethylrhodamine-labeled 10 kDa dextran dye (ThermoFisher D1816) in 1× PBS. The brains were rinsed again twice with 1× PBS and mounted on a glass slide using FluorSave (EMD Millipore). A Zeiss Confocal microscope was quickly used to image the slides.

Immunofluorescence quantification

The Sty and P-ERK fluorescence intensities were measured after selecting individual glial cell nuclei in multiple brains using the imageJ software (NIH). The average Sty (70 nuclei) and P-ERK (171 nuclei) intensities in the control *repo>+* glia nuclei were determined and compared to that in the *repo>Ama*^{RNAi} and *repo>Ama* glia nuclei to measure the relative fluorescent intensities of each immunostaining.

Tissue dissociation and Drop-seq

The dissociation protocol uses both collagenase (Sigma C9891) resuspended in 10× Krebs-Ringer with Ca^{2+} solution and 10× trypsin-EDTA (Sigma 59418C). The EDTA partially inhibits the collagenase to minimize tissue damage. Ten to fifteen third-instar brains were dissected in 30 min in 1× PBS on ice then transferred to a 1.5 ml microcentrifuge tube and spun down at 5000 rpm (~2000 ***g***) 4°C for 5 min. The brains were washed with Rinaldini solution and spundown at 5000 rpm (~2000 ***g***) 4°C for 5 min. While washing, the pellet remained carefully submerged to prevent the tissues from being pipetted up and sticking to the pipette tip. A digestion mix consisting of 1× trypsin and 2.5 mg/ml collagenase in Rinaldini's solution (500 µl) was added to resuspend the pelleted tissues. The microcentrifuge tube was oriented horizontally (to maximize the mechanical digestion and dissociation mix movement in the tube) on a shaker at 225 rpm for 45 min to an hour. The microcentrifuge tube was flicked every 10 min during the digestion step. The tube was spun down at 5000 rpm (~2000 ***g***) 4°C for 5 min before and between each following step: rinsing with 1× PBS with 0.01% BSA, rinsing with 1× PBS and resuspending cells in 60–100 µl 1× PBS. This protocol results in single cells and less than 5% clumps. The Drop-seq protocol was performed on the single-cell suspension as previously described (Ariss et al., 2018).

scRNA-seq alignment

Drop-seq data was analyzed using the pipeline wrapped in DropSeqPipe (version 0.5) (https://github.com/Hoohm/dropSeqPipe). This is based on

Drop-seq core computational pipeline described in 'Drop-seq_Alignment_Cookbook.pdf' version 2.0.0 on 9-28-18 (http://mccarrolllab.com/dropseq/) and the Drop-seq tools (version-2.3.0) was used to process the single-cell RNA-seq Illumina paired end raw sequences (FastQ files). STAR aligner was used to align the raw sequences against the *Drosophila melanogaster* genome version BDGP6 (Ensembl gene model version 90). The quality of reads and mapping were examined with the FastQC program (v0.11.8) (https://www.bioinformatics.babraham.ac.uk/projects/fastqc/) and poor quality reads (below 20) were eliminated before mapping.

The digital gene expression (DGE) was generated using the Drop-seq alignment protocol. The number of cells extracted from aligned BAM file is based on the knee plot, which extracts the number of reads per cell, then plotting the cumulative distribution of reads and selecting the knee of the distribution.

Cell clustering and single-cell analysis

The DGE files were subjected to Seurat (version 3.0.0) single-cell analysis to generate computational figures, such as dot plots, feature plots, UMAP and violin plots in R software (version 3.5.3). The standard Seurat workflow was followed, and we filtered the low-quality cells and outlier cells with a high gene number (min. gene cutoff=200 and max. gene cutoff=3000). The first 20 principle components were selected to run the UMAP with a resolution of 0.5 for the analyses of brains and a resolution 1.2 for the supervised glial cell analyses. The *repo>+*, *repo>Ama*^{RNAi} combined supervised glia analysis was performed using the cell barcodes listed in Table S7. The population labeled as 'other' display high levels of ribosomal genes and, therefore, considered to represent low quality cells.

Human cell lines

U251 cells were gifted by Nissim Hay (Department of Biochemistry & Molecular Genetics, University of Illinois at Chicago, USA) and T98G cells were gifted by Elizaveta Benevolenskaya (Department of Biochemistry & Molecular Genetics, University of Illinois at Chicago, USA). 293FT cells were acquired from Thermo Fisher. Both GBM cell lines were grown in MEM (Corning 10-010-CV) and 293FT were grown in DMEM (Corning 10-017-CV). All media were supplemented with 10% FBS (Gemini) and 1% penicillin-streptomycin (Corning 30-002-Cl). U251 cells were transduced with non-targeting (NT) or LSAMP shRNAs that were stably expressed. For immunoblotting experiments, 800,000 cells were split onto 6 cm plates and harvested 24 h later. T98G cells were transduced with a doxycycline-inducible shRNA targeting LSAMP. Following transduction, T98G cells were grown in medium with 10% tet-free FBS (Gemini). For immunoblotting experiments, 300,000 cells were plated onto 6 cm plates with the corresponding amount of doxycycline (sigma) added and grown for 72 h before harvesting. All conditions had 0.15% DMSO. Results from replicates are available upon request.

Plasmids and lentiviral production and transduction

Stably expressed shRNA plasmids, plko.1 empty vector and non-target (NT), were purchased from Sigma. The pTIP doxycycline inducible shRNA plasmid was a gift from Marcus Peter (xxx dept., institute, country xxx). The LSAMP-specific shRNA cloned into each plasmid was: 5′-CCGGCAAGTTTACTTGATCGTACAA-3′. For lentiviral production, 6×10^6 293FT cells were reverse transfected with 9 µg Virapower (Thermo Fisher) and 3 µg of the corresponding shRNA vector in 36 µl of Lipofectamine. The medium was changed 16 h after transfection, and 6 ml of viral particles was collected twice before filtering through a 0.45 µm filter. Cells were transduced with 2 ml of viral supernatant diluted in 2 ml of complete medium supplemented with 8 µg/ml of polybrene (Sigma 107689). 48 h after transduction, cells were selected in 1 µg/ml of puromycin (ACROS organics 227420100) for 5 days. (Putzbach et al., 2017).

Immunoblotting

At the indicated time point, cells were washed twice with cold PBS on ice. Then, 100 µl of 1× RIPA (Cell Signaling #9806S), supplemented with phosphatase and protease inhibitor tablets (Peirce A32957 and A32953), was added to each plate for 5 min before scraping and collecting into 1.5 ml Eppendorf tubes. Lysates were vortexed on high for 10 s every 10 min for 30 min before centrifuging at 13,000 ***g*** for 10 min. The lysate supernatant was collected, and the protein concentration was determined with the Bradford Method (Bio-Rad). A total of 20–30 µg of protein was loaded for each sample and ran via standard electrophoresis on a 10% polyacrylamide gel and transferred for 75 min at 115 v onto PVDF membranes. Membranes were then blocked in 5% milk Tris-buffered saline with 0.1% Tween 20 (TBS-T) with for 1 h. Primary antibodies were incubated on a shaker over night at 4°C in 2.5% milk in TBS-T. Membranes were washed 3× in TBS-T before the corresponding secondary antibody (1:3000) was added for 1 h at room temperature. Membranes were washed 3× in TBS-T before developing on an Azure cSeries with chemiluminescence. Primary antibodies used were against: LSAMP (Abcam ab64427; 1:500), SPRY2 (Millipore #07-524; 1:1000), GAPDH (Cell Signaling D16H11; 1:5000) and vinculin (Sigma V9131; 1:5000). The relative densitometries were determined using Image Studio Lite Ver 5.2.

TCGA – cBioportal

Glioblastoma TCGA PanCancer Atlas patient samples were selected in cBioportal (https://www.cbioportal.org/) (Gao et al., 2013; Cerami et al., 2012). The *LSAMP* and *SPRY2* heatmap was generated using the 'OncoPrint' tab in cBioportal.

Using the 'Custom Selection' in cBioportal, GBM patients with EGFR mutations were split into two groups based on the median LSAMP expression (LSAMP high versus LSAMP low) in the 'Groups' tab. The survivability was then plotted. The same was achieved using GBM patients with EGFR amplifications that were split into two groups based on the first and fourth quartiles in LSAMP expression (LSAMP high versus LSAMP low).

Acknowledgements

The authors are grateful to Renee Read, Vicki Losick, and Teresa Orenic for sharing *Drosophila* stocks as well as Roland Bainton and Mark Krasnow, James Skeath, and István Ando for recommending and sharing antibodies and Elizaveta Benevolenskaya for sharing cell lines. We thank the Developmental Studies Hybridoma Bank for the antibodies and Bloomington Stock Center at Indiana University for *Drosophila* stocks.

Competing interests

The authors declare no competing or financial interests.

Author contributions

Conceptualization: M.M.A., M.V.F.; Software: A.B.M.M.K.I.; Formal analysis: A.B.M.M.K.I., M.M.A.; Investigation: M.M.A., A.R.T.; Writing - original draft: M.M.A.; Writing - review & editing: M.V.F.; Visualization: M.M.A.; Supervision: N.H., M.V.F.; Project administration: M.V.F.; Funding acquisition: A.R.T., N.H., M.V.F.

Funding

This work is funded by the National Institutes of Health grants R35GM131707 to M.V.F., R01AG016927, R01CA090764, R01CA206167 to N.H. and F30CA225058 to A.R.T.; the U.S. Department of Veterans Affairs grants BX000733 and IK6BX004602 to N.H. Deposited in PMC for release after 12 months.

Data availability

All raw sequencing data are deposited in the Gene Expression Omnibus (GEO) database under accession code GSE147688.

Supplementary information

Supplementary information available online at
https://jcs.biologists.org/lookup/doi/10.1242/jcs.250837.supplemental

References

Akeel, M., McNamee, C. J., Youssef, S. and Moss, D. (2011). DIgLONs inhibit initiation of neurite outgrowth from forebrain neurons via an IgLON-containing receptor complex. *Brain Res.* **1374**, 27-35. doi:10.1016/j.brainres.2010.12.028

Ariss, M. M., Islam, A. B. M. M. K., Critcher, M., Zappia, M. P. and Frolov, M. V. (2018). Single cell RNA-sequencing identifies a metabolic aspect of apoptosis in Rbf mutant. *Nat. Commun.* **9**, 1-13. doi:10.1038/s41467-018-07540-z

Avet-Rochex, A., Kaul, A. K., Gatt, A. P., McNeill, H. and Bateman, J. M. (2012). Concerted control of gliogenesis by InR/TOR and FGF signalling in the Drosophila post-embryonic brain. *Development* **139**, 2763-2772. doi:10.1242/dev.074179

Babatz, F., Naffin, E. and Klämbt, C. (2018). The Drosophila blood-brain barrier adapts to cell growth by unfolding of pre-existing septate junctions. *Dev. Cell* **47**, 697-710.e3. doi:10.1016/j.devcel.2018.10.002

Bainton, R. J., Tsai, L. T.-Y., Schwabe, T., DeSalvo, M., Gaul, U. and Heberlein, U. (2005). moody encodes two GPCRs that regulate cocaine behaviors and blood-brain barrier permeability in Drosophila. *Cell* **123**, 145-156. doi:10.1016/j.cell.2005.07.029

Bangi, E., Murgia, C., Teague, A. G. S., Sansom, O. J. and Cagan, R. L. (2016). Functional exploration of colorectal cancer genomes using Drosophila. *Nat. Commun.* **7**, 13615. doi:10.1038/ncomms13615

Butchar, J. P., Cain, D., Manivannan, S. N., McCue, A. D., Bonanno, L., Halula, S., Truesdell, S., Austin, C. L., Jacobsen, T. L. and Simcox, A. (2012). New negative feedback regulators of Egfr signaling in Drosophila. *Genetics* **191**, 1213-1226. doi:10.1534/genetics.112.141093

Cerami, E., Gao, J., Dogrusoz, U., Gross, B. E., Sumer, S. O., Aksoy, B. A., Jacobsen, A., Byrne, C. J., Heuer, M. L., Larsson, E. et al. (2012). The cBio cancer genomics portal: an open platform for exploring multidimensional cancer genomics data. *Cancer Discov.* **2**, 401-404. doi:10.1158/2159-8290.CD-12-0095

Chatterjee, D. and Deng, W. M. (2019). Drosophila Model in Cancer: An Introduction. *Adv Exp. Med. Biol.* **1167**, 1-14. doi:10.1007/978-3-030-23629-8_1

DeSalvo, M. K., Hindle, S. J., Rusan, Z. M., Orng, S., Eddison, M., Halliwill, K. and Bainton, R. J. (2014). The Drosophila surface glia transcriptome: evolutionary conserved blood-brain barrier processes. *Front. Neurosci.* **8**, 346. doi:10.3389/fnins.2014.00346

Doherty, J., Logan, M. A., Taşdemir, Ö. E. and Freeman, M. R. (2009). Ensheathing glia function as phagocytes in the adult Drosophila brain. *J. Neurosci.* **29**, 4768-4781. doi:10.1523/JNEUROSCI.5951-08.2009

Evans, C. J., Olson, J. M., Ngo, K. T., Kim, E., Lee, N. E., Kuoy, E., Patananan, A. N., Sitz, D., Tran, P., Do, M. T. et al. (2009). G-TRACE: rapid Gal4-based cell lineage analysis in Drosophila. *Nat. Methods* **6**, 603. doi:10.1038/nmeth.1356

Franzdóttir, S. R., Engelen, D., Yuva-Aydemir, Y., Schmidt, I., Aho, A. and Klämbt, C. (2009). Switch in FGF signalling initiates glial differentiation in the Drosophila eye. *Nature* **460**, 758-761. doi:10.1038/nature08167

Fremion, F., Darboux, I., Diano, M., Hipeau–Jacquotte, R., Seeger, M. A. and Piovant, M. (2000). Amalgam is a ligand for the transmembrane receptor neurotactin and is required for neurotactin–mediated cell adhesion and axon fasciculation in Drosophila. *EMBO J.* **19**, 4463-4472. doi:10.1093/emboj/19.17.4463

Furnari, F. B., Fenton, T., Bachoo, R. M., Mukasa, A., Stommel, J. M., Stegh, A., Hahn, W. C., Ligon, K. L., Louis, D. N., Brennan, C. et al. (2007). Malignant astrocytic glioma: genetics, biology, and paths to treatment. *Genes Dev.* **21**, 2683-2710. doi:10.1101/gad.1596707

Gao, J., Aksoy, B. A., Dogrusoz, U., Dresdner, G., Gross, B., Sumer, S. O., Sun, Y., Jacobsen, A., Sinha, R., Larsson, E. et al. (2013). Integrative analysis of complex cancer genomics and clinical profiles using the cBioPortal. *Sci. Signal.* **6**, pl1. doi:10.1126/scisignal.2004088

Goto, A., Kadowaki, T. and Kitagawa, Y. (2003). Drosophila hemolectin gene is expressed in embryonic and larval hemocytes and its knock down causes bleeding defects. *Dev. Biol.* **264**, 582-591. doi:10.1016/j.ydbio.2003.06.001

Hacohen, N., Kramer, S., Sutherland, D., Hiromi, Y. and Krasnow, M. A. (1998). sprouty encodes a novel antagonist of FGF signaling that patterns apical branching of the Drosophila airways. *Cell* **92**, 253-263. doi:10.1016/S0092-8674(00)80919-8

Haghverdi, L., Lun, A. T. L., Morgan, M. D. and Marioni, J. C. (2018). Batch effects in single-cell RNA-sequencing data are corrected by matching mutual nearest neighbors. *Nat. Biotechnol.* **36**, 421-427. doi:10.1038/nbt.4091

Hanafusa, H., Torii, S., Yasunaga, T. and Nishida, E. (2002). Sprouty1 and Sprouty2 provide a control mechanism for the Ras/MAPK signalling pathway. *Nat. Cell Biol.* **4**, 850-858. doi:10.1038/ncb867

Hausott, B. and Klimaschewski, L. (2019). Sprouty2—A novel therapeutic target in the nervous system? *Mol. Neurobiol.* **56**, 3897-3903. doi:10.1007/s12035-018-1338-8

Impagnatiello, M.-A., Weitzer, S., Gannon, G., Compagni, A., Cotten, M. and Christofori, G. (2001). Mammalian sprouty-1 and-2 are membrane-anchored phosphoprotein inhibitors of growth factor signaling in endothelial cells. *J. Cell Biol.* **152**, 1087-1098. doi:10.1083/jcb.152.5.1087

Jarvis, L. A., Toering, S. J., Simon, M. A., Krasnow, M. A. and Smith-Bolton, R. K. (2006). Sprouty proteins are in vivo targets of Corkscrew/SHP-2 tyrosine phosphatases. *Development* **133**, 1133-1142. doi:10.1242/dev.02255

Kresse, S. H., Ohnstad, H. O., Paulsen, E. B., Bjerkehagen, B., Szuhai, K., Serra, M., Schaefer, K.-L., Myklebost, O. and Meza-Zepeda, L. A. (2009). LSAMP, a novel candidate tumor suppressor gene in human osteosarcomas, identified by array comparative genomic hybridization. *Genes Chromosomes Cancer* **48**, 679-693. doi:10.1002/gcc.20675

Kubick, N., Brösamle, D. and Mickael, M.-E. (2018). Molecular evolution and functional divergence of the IgLON family. *Evol. Bioinform.* **14**, 1176934318775081. doi:10.1177/1176934318775081

Kurucz, É., Váczi, B., Márkus, R., Laurinyecz, B., Vilmos, P., Zsámboki, J., Csorba, K., Gateff, E., Hultmark, D. and Andó, I. (2007). Definition of Drosophila hemocyte subsets by cell-type specific antigens. *Acta Biol. Hung.* **58**, 95-111. doi:10.1556/ABiol.58.2007.Suppl.8

Levine, B. D. and Cagan, R. L. (2016). Drosophila lung cancer models identify trametinib plus statin as candidate therapeutic. *Cell Rep.* **14**, 1477-1487. doi:10.1016/j.celrep.2015.12.105

Liu, S. and Trapnell, C. (2016). Single-cell transcriptome sequencing: recent advances and remaining challenges. *F1000Research* **5**, 182. doi:10.12688/f1000research.7223.1

Macosko, E. Z., Basu, A., Satija, R., Nemesh, J., Shekhar, K., Goldman, M., Tirosh, I., Bialas, A. R., Kamitaki, N., Martersteck, E. M. et al. (2015). Highly parallel genome-wide expression profiling of individual cells using nanoliter droplets. *Cell* **161**, 1202-1214. doi:10.1016/j.cell.2015.05.002

Masoumi-Moghaddam, S., Amini, A. and Morris, D. L. (2014). The developing story of Sprouty and cancer. *Cancer Metastasis Rev.* **33**, 695-720. doi:10.1007/s10555-014-9497-1

Omoto, J. J., Yogi, P. and Hartenstein, V. (2015). Origin and development of neuropil glia of the Drosophila larval and adult brain: two distinct glial populations derived from separate progenitors. *Dev. Biol.* **404**, 2-20. doi:10.1016/j.ydbio.2015.03.004

O'Neill, E. M., Rebay, I., Tjian, R. and Rubin, G. M. (1994). The activities of two Ets-related transcription factors required for Drosophila eye development are modulated by the Ras/MAPK pathway. *Cell* **78**, 137-147. doi:10.1016/0092-8674(94)90580-0

Osman, D., Gobert, V., Ponthan, F., Heidenreich, O., Haenlin, M. and Waltzer, L. (2009). A Drosophila model identifies calpains as modulators of the human leukemogenic fusion protein AML1-ETO. *Proc. Natl Acad. Sci. USA* **106**, 12043-12048. doi:10.1073/pnas.0902449106

Pagliarini, R. A. and Xu, T. (2003). A genetic screen in Drosophila for metastatic behavior. *Science* **302**, 1227-1231. doi:10.1126/science.1088474

Papalexi, E. and Satija, R. (2018). Single-cell RNA sequencing to explore immune cell heterogeneity. *Nat. Rev. Immunol.* **18**, 35. doi:10.1038/nri.2017.76

Pereanu, W., Spindler, S., Cruz, L. and Hartenstein, V. (2007). Tracheal development in the Drosophila brain is constrained by glial cells. *Dev. Biol.* **302**, 169-180. doi:10.1016/j.ydbio.2006.09.022

Perrimon, N. (1994). Signalling pathways initiated by receptor protein tyrosine kinases in Drosophila. *Curr. Opin. Cell Biol.* **6**, 260-266. doi:10.1016/0955-0674(94)90145-7

Putzbach, W., Gao, Q. Q., Patel, M., Van Dongen, S., Haluck-Kangas, A., Sarshad, A. A., Bartom, E. T., Kim, K.-Y. A., Scholtens, D. M., Hafner, M. et al. (2017). Many si/shRNAs can kill cancer cells by targeting multiple survival genes through an off-target mechanism. *eLife* **6**, e29702. doi:10.7554/eLife.29702

Ray, A., Speese, S. D. and Logan, M. A. (2017). Glial Draper rescues Aβ toxicity in a Drosophila model of Alzheimer's Disease. *J. Neurosci.* **37**, 11881-11893. doi:10.1523/JNEUROSCI.0862-17.2017

Read, R. D. (2018). Pvr receptor tyrosine kinase signaling promotes post-embryonic morphogenesis, and survival of glia and neural progenitor cells in Drosophila. *Development* **145**, dev164285. doi:10.1242/dev.164285

Read, R. D., Cavenee, W. K., Furnari, F. B. and Thomas, J. B. (2009). A drosophila model for EGFR-Ras and PI3K-dependent human glioma. *PLoS Genet.* **5**, e1000374. doi:10.1371/journal.pgen.1000374

Regad, T. (2015). Targeting RTK signaling pathways in cancer. *Cancers* **7**, 1758-1784. doi:10.3390/cancers7030860

Rubin, C., Litvak, V., Medvedovsky, H., Zwang, Y., Lev, S. and Yarden, Y. (2003). Sprouty fine-tunes EGF signaling through interlinked positive and negative feedback loops. *Curr. Biol.* **13**, 297-307. doi:10.1016/S0960-9822(03)00053-8

Sasse, S., Neuert, H. and Klämbt, C. (2015). Differentiation of Drosophila glial cells. *Wiley Interdiscipl. Rev. Dev. Biol.* **4**, 623-636. doi:10.1002/wdev.198

Seeger, M. A., Haffley, L. and Kaufman, T. C. (1988). Characterization of amalgam: a member of the immunoglobulin superfamily from Drosophila. *Cell* **55**, 589-600. doi:10.1016/0092-8674(88)90217-6

Simon, M. A., Bowtell, D. D., Dodson, G. S., Laverty, T. R. and Rubin, G. M. (1991). Ras1 and a putative guanine nucleotide exchange factor perform crucial steps in signaling by the sevenless protein tyrosine kinase. *Cell* **67**, 701-716. doi:10.1016/0092-8674(91)90065-7

Strigini, M., Cantera, R., Morin, X., Bastiani, M. J., Bate, M. and Karagogeos, D. (2006). The IgLON protein Lachesin is required for the blood–brain barrier in Drosophila. *Mol. Cell. Neurosci.* **32**, 91-101. doi:10.1016/j.mcn.2006.03.001

Stuart, T., Butler, A., Hoffman, P., Hafemeister, C., Papalexi, E., Mauck, W. M., III, Hao, Y., Stoeckius, M., Smibert, P. and Satija, R. (2019). Comprehensive integration of single-cell data. *Cell* **177**, 1888-1902.e21. doi:10.1016/j.cell.2019.05.031

Sugimoto, C., Morita, S. and Miyata, S. (2012). Overexpression of IgLON cell adhesion molecules changes proliferation and cell size of cortical astrocytes. *Cell Biochem. Funct.* **30**, 400-405. doi:10.1002/cbf.2813

Sweeney, M. D., Sagare, A. P. and Zlokovic, B. V. (2018). Blood–brain barrier breakdown in Alzheimer disease and other neurodegenerative disorders. *Nat. Rev. Neurol.* **14**, 133. doi:10.1038/nrneurol.2017.188

Thurmond, J., Goodman, J. L., Strelets, V. B., Attrill, H., Gramates, L. S., Marygold, S. J., Matthews, B. B., Millburn, G., Antonazzo, G., Trovisco, V. et al. (2019). FlyBase 2.0: the next generation. *Nucleic Acids Res.* **47**, D759-D765. doi:10.1093/nar/gky1003

Unhavaithaya, Y. and Orr-Weaver, T. L. (2012). Polyploidization of glia in neural development links tissue growth to blood–brain barrier integrity. *Genes Dev.* **26**, 31-36. doi:10.1101/gad.177436.111

Volkenhoff, A., Weiler, A., Letzel, M., Stehling, M., Klämbt, C. and Schirmeier, S. (2015). Glial glycolysis is essential for neuronal survival in Drosophila. *Cell Metab.* **22**, 437-447. doi:10.1016/j.cmet.2015.07.006

Wagner, A., Regev, A. and Yosef, N. (2016). Revealing the vectors of cellular identity with single-cell genomics. *Nat. Biotechnol.* **34**, 1145. doi:10.1038/nbt.3711

Xie, X., Gilbert, M., Petley-Ragan, L. and Auld, V. J. (2014). Loss of focal adhesions in glia disrupts both glial and photoreceptor axon migration in the Drosophila visual system. *Development* **141**, 3072-3083. doi:10.1242/dev.101972

Yeh, P.-A., Liu, Y.-H., Chu, W.-C., Liu, J.-Y. and Sun, Y. H. (2018). Glial expression of disease-associated poly-glutamine proteins impairs the blood–brain barrier in Drosophila. *Hum. Mol. Genet.* **27**, 2546-2562. doi:10.1093/hmg/ddy160

Yildirim, K., Petri, J., Kottmeier, R. and Klämbt, C. (2019). Drosophila glia: few cell types and many conserved functions. *Glia* **67**, 5-26. doi:10.1002/glia.23459

Yoshida, S., Soustelle, L., Giangrande, A., Umetsu, D., Murakami, S., Yasugi, T., Awasaki, T., Ito, K., Sato, M. and Tabata, T. (2005). DPP signaling controls development of the lamina glia required for retinal axon targeting in the visual system of Drosophila. *Development* **132**, 4587-4598. doi:10.1242/dev.02040